



Jomo Kenyatta University of Agriculture and Technology

College of Engineering and Technology

School of Mechanical, Materials, and Manufacturing Engineering

Department of Mechatronic Engineering

---

# **Design and Fabrication of an Automated Discharge Collection Unit for the Synthetic Hydro-experimental Machine.**

**FYP-18-03**

## **FINAL REPORT**

**Juma Joel Mwimali (ENM221-0060/2017)**

**Kipng'eno Erick (ENM221-0068/2017)**

**Supervisor**

**Dr. Anthony Muchiri**

**December, 2022**

---

Submitted in partial fulfillment of the requirements for the degree of Bachelor of Science in Mechatronic Engineering at Jomo Kenyatta University of Agriculture and Technology, 2022

## Declaration

We hereby declare that the work contained in this report is original, researched and documented by the undersigned students. It has not been used or presented elsewhere in any form for award of any academic qualification or otherwise. Any material obtained from other parties have been duly acknowledged. We have ensured that no violation of copyright or intellectual property rights have been committed.

1. Juma Joel Mwimali

Signature..... Date.....

2. Kipng'eno Erick

Signature..... Date.....

Approved by:

**Supervisor:** Dr. Anthony Muchiri

Signature..... Date.....

**Technologist:** Mr. Mbugua

Signature..... Date.....

## Abstract

The synthetic hydro-experimental machine used for fluid mechanics experiments in the fluids lab at JKUAT uses a manual mechanical system for the collection of the discharge during experiments such as the determination of the coefficient of discharge of the Venturi and the orifice. During such experiments, the user is required to turn the main discharge ball valve in steps determined by human intuition, and for every step, they are required to slide a metallic diverter to collect the discharge to a separate tank, and at the same time, to start measuring the temperature of the discharge, and the timer using an analog stopwatch. This synchronism is necessary for precise data in the computation of the fluid flow properties but cannot be achieved by humans.

The design and fabrication of an automated discharge collection unit intended to reduce human error by approximately 10% have been outlined in this report. The design was modularised into three units; a discharge flow control unit, a discharge handling unit, and an interface and a control unit. The discharge flow control unit was designed to control the main ball valve in steps of less than  $1^{\circ}$  using a servo motor and divert the flow in less than 1.5 seconds using a linear actuator. The discharge handling unit was also designed with a tank that can collect up to 25 kg of discharge. The tank was also fitted with automated temperature and weight measurement units. The interface was designed on a touch LCD running on an STM32 microcontroller.

This automation results in a reduction of the gross error by 8.213 %.

Abstract	III
----------	-----

---

## Contents

<b>Declaration</b>	I
<b>Abstract</b>	II
<b>Table of Contents</b>	VI
<b>List of Figures</b>	VI
<b>Nomenclature</b>	IX
<b>1 Introduction</b>	1
1.1 Background	1
1.2 Problem statement	1
1.3 Objectives	2
1.3.1 Main objective	2
1.3.2 Specific objectives	2
1.3.3 Expected outcomes	2
1.4 Justification	3
<b>2 Literature Review</b>	4
2.1 Introduction	4
2.1.1 Gate Valve	4
2.1.2 Diverter	5
2.1.3 Temperature measurement unit	5
2.1.4 Pressure measurement	5
2.1.5 Weight measurement unit	5
2.2 Existing Technologies	6
2.2.1 Computational Fluid Dynamics	6
2.2.2 Analytical Predictions	9
2.3 Related Works	11

2.3.1	Electromagnetic activation . . . . .	11
2.3.2	Pneumatic Control . . . . .	12
2.4	Summary . . . . .	13
2.5	Gap analysis . . . . .	13
<b>3</b>	<b>Methodology . . . . .</b>	<b>15</b>
3.1	Discharge Flow Control Unit . . . . .	15
3.1.1	Mechanical Design and Fabrication . . . . .	15
3.1.2	Material selection . . . . .	25
3.1.3	Design Modifications . . . . .	26
3.1.4	Electrical and Electronics . . . . .	27
3.2	Discharge handling unit . . . . .	31
3.2.1	Mechanical design and fabrication . . . . .	31
3.2.2	Electrical and electronics . . . . .	37
3.3	Interface and control unit . . . . .	40
3.3.1	Interface and control sub-unit . . . . .	40
3.3.2	Software and controller sub-unit . . . . .	46
<b>4</b>	<b>Results and Discussion . . . . .</b>	<b>51</b>
4.1	Final Design . . . . .	51
4.2	The Discharge Flow Control unit . . . . .	52
4.3	The discharge handling unit . . . . .	54
4.4	Electrical and Electronics Unit . . . . .	55
4.5	Final Assembly . . . . .	56
4.6	Experiments Conducted . . . . .	57
4.6.1	Experiment 1 . . . . .	58
4.6.2	Experiment 1 . . . . .	59
4.6.3	Experiment 2 . . . . .	60
4.6.4	Experiment 3 . . . . .	61

<b>5 Conclusion . . . . .</b>	<b>63</b>
5.1 Recommendation . . . . .	63
<b>References . . . . .</b>	<b>64</b>
<b>Appendices . . . . .</b>	<b>66</b>
<b>A Appendix . . . . .</b>	<b>66</b>
A.0.1 Budget . . . . .	66
A.0.2 Computation of the coefficient of discharge of the venturi meter . .	66
A.0.3 Semester 1 & 2 Time Plan . . . . .	68

## List of Figures

Figure 2.1	Test loop schematic . . . . .	7
Figure 2.2	Experimental setup . . . . .	8
Figure 2.3	Venturi Meter . . . . .	9
Figure 2.4	Sampler actuation mechanism . . . . .	11
Figure 2.5	Dispensing mechanism . . . . .	12
Figure 3.1	Servo motor bracket . . . . .	16
Figure 3.2	3D printed Servo Holder . . . . .	17
Figure 3.3	LA-T8 Holder . . . . .	17
Figure 3.4	3D printed LA-T8 holder . . . . .	18
Figure 3.5	Top Strap . . . . .	19
Figure 3.6	Bottom Strap . . . . .	20
Figure 3.7	3D printed top and bottom straps . . . . .	21
Figure 3.8	Interface . . . . .	22
Figure 3.9	Diversion Flap . . . . .	23
Figure 3.10	Mounting Rod . . . . .	24
Figure 3.11	Mounting Rod . . . . .	25
Figure 3.12	Link1 . . . . .	26
Figure 3.13	Link2 . . . . .	27
Figure 3.14	10Kg MG996R Servo Motor . . . . .	28
Figure 3.15	20Kg Metal Gear Digital Servo . . . . .	29
Figure 3.16	LA-T8 Electromagnet Linear Actuator . . . . .	30
Figure 3.17	Electrical Circuit Schematic . . . . .	31
Figure 3.18	Horizontal Cylindrical tank . . . . .	32
Figure 3.19	Cylindrical tank support frame . . . . .	33
Figure 3.20	Fabricated tank . . . . .	34
Figure 3.21	Tank support frame . . . . .	34
Figure 3.22	Cushion/suspension rubber . . . . .	35

Figure 3.23 Mounted collection tank . . . . .	36
Figure 3.24 Fabricated discharge handling unit . . . . .	37
Figure 3.25 Strain-type load cells . . . . .	38
Figure 3.26 Collection tank with load cells . . . . .	38
Figure 3.27 Load cell connection . . . . .	39
Figure 3.28 DS18B20 temperature probe . . . . .	40
Figure 3.29 Home screen . . . . .	42
Figure 3.30 Screen 1 . . . . .	42
Figure 3.31 Screen 2 . . . . .	43
Figure 3.32 Application control flow . . . . .	45
Figure 3.33 Load cells circuit . . . . .	47
Figure 3.34 STM32 connected with LCD . . . . .	47
Figure 3.35 Firmware architecture . . . . .	48
Figure 3.36 Desktop application . . . . .	50
Figure 4.1 Unit Exploded view . . . . .	51
Figure 4.2 Controls for the flow control . . . . .	52
Figure 4.3 Discharge Flow Control Unit . . . . .	53
Figure 4.4 Discharge Handling Unit . . . . .	54
Figure 4.5 Electrical Assembly . . . . .	55
Figure 4.6 User Interface Mounted . . . . .	56
Figure 4.7 Finally Assembly . . . . .	57
Figure 4.8 Manual Experiment . . . . .	59
Figure 4.9 Experiment1 . . . . .	60
Figure 4.10 Experiment2 . . . . .	61
Figure 4.11 Experiment3 . . . . .	62

## List of Tables

Table 2.1	Calculated $C_d$	7
Table 2.2	Results	8
Table 3.1	MG996R Servo motor specifications	28
Table 3.2	DS8120 Servo motor specifications	29
Table 3.3	LA-T8 Micro-linear Actuator technical specifications	30
Table 4.1	Manual Experiment	58
Table 4.2	Experiment 1	59
Table 4.3	Experiment 2	60
Table 4.4	Experiment 3	61
Table A.1	Budget	66
Table A.2	Semester 1 timeplan	68
Table A.3	Semester 2 Timeplan	69
Table A.4	Production Plan	70

## Nomenclature

API Application Programming Interface

CFD Computational Fluid Dynamics

FSMC Flexible Static Memory Controller

GPIO General Purpose Input and Output Pins

GPIO General Purpose Input Output

MAWS Marine Automatic Water Sampler

MOSFET Metal Oxide Field Effect Transistor

RTOS Real Time Operating System

SKE Single Kernel Estimate

UMV Unmanned Marine Vehicle

# 1 Introduction

## 1.1 Background

Fluid flow measurement involves the measurement of the properties of a smooth and uninterrupted stream of flowing particles that conform to a pipe. These flow properties include the coefficient of discharge, mass flow rate, fluid velocity, differential pressure, and conductivity coefficients [1]. They are altered and measured by flow measuring devices such as the Venturi, the Orifice, turbine flow meters and rotameters [2]. These measurements are finally related to the flow using the Bernoulli's equation.

The Synthetic Hydro-Experimental machine, currently installed in JKUAT, is a configurable machine with these flow meters. This machine is used to conduct experiments to establish relationships between the fluid flow properties and the behavior of the flow. It has a lift pump, gate valves, alcohol manometers, pressure gauges, a Pelton turbine, a Venturi, an orifice, and water reservoirs. During experiments, the lift pump is turned on, and the discharge valve is fully opened to establish a steady flow. The discharge valve is then closed. The valve is opened in small steps depending on the number of steps required. For each step, the discharge is collected, and its temperature is measured within a specific time interval. Finally, the weight of the collected discharge is also measured.

## 1.2 Problem statement

In fluid flow experiments utilizing the Venturi and the orifice to establish the coefficient of discharge, the discharge steps must be precisely opened, time and temperature measurements must be made concurrently with discharge collection so as to achieve values that are within a reasonable range. The Synthetic Hydro-Experimental machine now in use at JKUAT to establish this relationship, however, is entirely mechanical, making it impossible for a human to do some of the simultaneous measurements. A ball valve regulates the flow rate in small intervals using human intuition, which can be imprecise. As a

result, with these discrepancies, the findings might frequently be outside of the acceptable range. Automating the discharge collection process can minimize the error in the results and still preserve the credibility of the experiment.

### **1.3 Objectives**

#### **1.3.1 Main objective**

To automate the discharge collection process for the Synthetic Hydro-Experimental machine.

#### **1.3.2 Specific objectives**

1. To design an automated discharge flow control unit that can turn the ball valve in steps of less than  $1^0$  and divert the flow in less than 1 second. Turning of less than  $1^0$  ensures more runs of experiment can be conducted.
2. To design and fabricate a discharge handling unit with automated weight, time and temperature measurements, and a discharge collection tank that can discharge within 2 seconds.
3. To design a graphical user interface and a robust control algorithm to integrate the units.

#### **1.3.3 Expected outcomes**

A unit with a discharge flow control mechanism that can turn in steps of less than  $1^0$ . Furthermore, to accurately regulate the flow of the discharge into either the collecting tank or into the main reservoir, the mechanism should be able to divert the flow from the pipeline in less than a second. The discharge should then be collected in a tank that can store up to  $0.02m^3$  of the discharge. A weight measurement device with a gauge factor

of more than 2 to be attached at the bottom of the collection tank. A graphical user interface that allows for the displaying of measurements in this case temperature, time and weight and control of operations

## 1.4 Justification

This automation will streamline the discharge collecting process while also ensuring the consistency and quality of the data collected in each phase of the fluid flow tests performed on the system. In contrast to the existing condition, such automation allows a single person to perform the experiment without significant effort. Furthermore, the automated system will also be modular, allowing it to be readily attached and detached from the main machine with few modifications.

## 2 Literature Review

### 2.1 Introduction

Fluid flow experiments involve determination of the flow velocity, the mass flow rate or volumetric flow rate. These experiments are used to familiarize the students with typical methods of flow measurement of an incompressible fluid and, at the same time demonstrate applications of the Bernoulli's equation. Thus, these experimental investigations require the application of measuring techniques to yield quantitative information on the relationship between pressure, temperature and local flow velocities.

The synthetic hydro-experimental machine employs the use of the venturi and the orifice meter in determining these fluid properties specifically the coefficient of discharge. It involves determining the relationship between a flowing fluid through a valve, the weight and temperature of the collected discharge. The machine comprises of four main parts; the diverter, gate valve, weight and temperature measurement unit. The measurement involves four main processes, discharge collection, diversion, weight and temperature measurement.

#### 2.1.1 Gate Valve

The valve is attached at the end of the pipeline immediately after the venturi and the orifice meter. It is used in flow rate control by either increasing or reducing the aperture at which the fluid flows. The experiment is conducted in several steps which is determined by opening and closing of the valve. At the start of the experiment, the valve is initially closed hence no fluid is collected. Depending on the required number of steps, the valve is then opened in small steps allowing the discharge to be collected for purposes of weight and temperature measurement.

### **2.1.2 Diverter**

After each step of the experiment, the collected fluid flows into the weight measurement unit through the help of a diverter. The diverter is used to direct the collected discharge into the weight measurement unit which is located at the periphery of the rig to avoid flowing back into the reservoir. The diverter is a mechanical device that is moved by hand.

### **2.1.3 Temperature measurement unit**

The temperature of the collected discharge is measured immediately after the fluid flows through the gate valve by use of a thermometer. This is to minimize the environmental effects, for instance the effects of the metallic diverters which would otherwise compromise on the temperature readings. The readings are measured and recorded after each step of the experiment.

### **2.1.4 Pressure measurement**

The differential manometers are attached just before and after both the venture and the orifice and is used to determine the pressure of the flowing fluid. These manometric readings are recorded after each and every step of the experiment.

### **2.1.5 Weight measurement unit**

The final part involves measuring the weight of the collected discharge. This is done by use of a measuring scale with loads attached to it. The above measurements are then used to establish the coefficient of discharge of the fluid.

## 2.2 Existing Technologies

Some advanced and even rudimentary technologies have been used in place of the Synthetic Hydro-Experimental machine for the determination of fluid flow properties. The technologies include :

### 2.2.1 Computational Fluid Dynamics

Computational fluid dynamics(CFD) is a powerful modelling and analysis technique that utilizes finite difference techniques to solve highly non-linear differential equation of pressure, energy, relative humidity, air temperature and velocity [3]. It can be used to model fluid flow in flow measurement devices.

Tukimin et al [4] in their study conducted a CFD analysis using an Single Kernel Estimate (SKE) turbulence model to determine the coefficient of discharge of a Venturi tube, and finally compared the results to those obtained from a physical experimental setup. The test loop shown in figure 2.1 was used both in a physical setup and a CFD model.

They designed a CFD model using the ANSYS Design Modeller software. The model consists of a Venturi tube, designed according to the standards ISO 5167:2003 [5], and a liquid and gas system. They did a physical experiment using the same test matrix used in the numerical simulation model. Finally, they computed the coefficient of discharge of the venturi using equation 2.1.

$$Cd = \frac{4m\sqrt{1 - \beta^4}}{\pi\varepsilon d^2\sqrt{200000D\rho_1\rho_1}} \quad (2.1)$$

The results obtained in 2.1 showed a difference of less than 1% between the  $C_d$  obtained from the two setups.

Tamhankar et al [6] also did a similar experiment using a CFD model designed in ANSYS Fluent 13.0 utilizing a Realizable k- $\epsilon$  turbulence model which is superior to a Standard

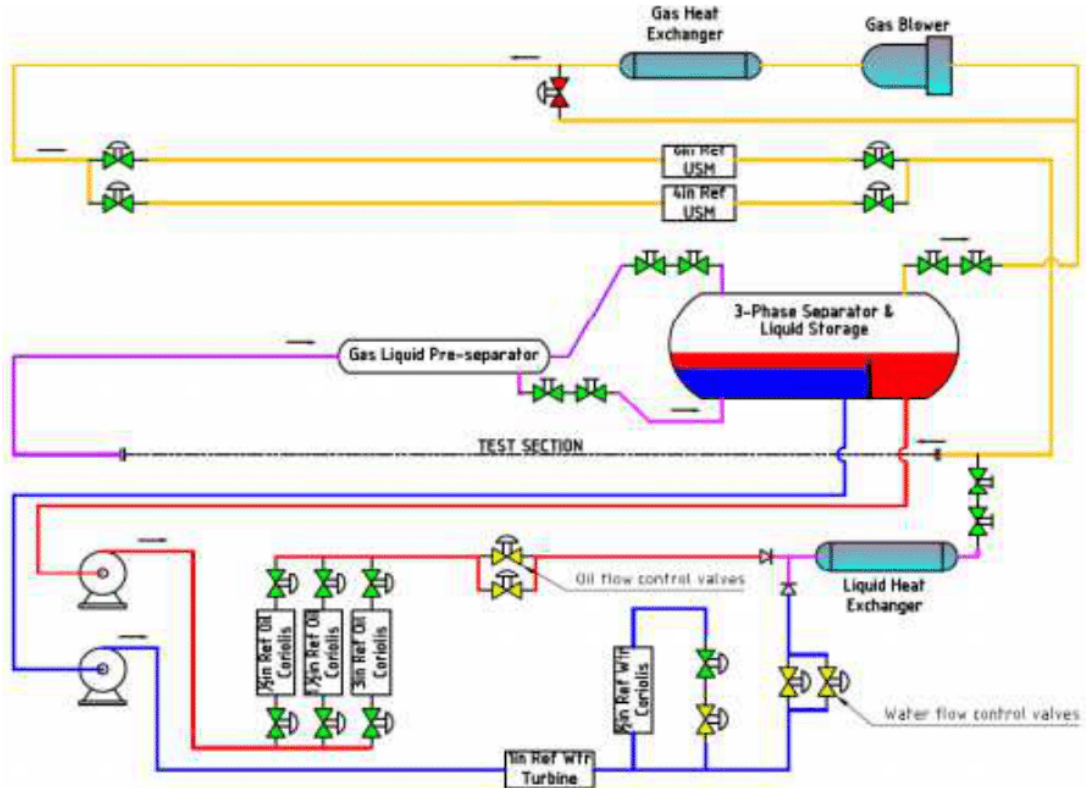


Figure 2.1: Test loop schematic by Tukimin et al [4]

Table 2.1: Calculated  $C_d$ 

Venturi under Test	Average Discharge Coefficient From experiment	Average Discharge Coefficient From CFD post
Venturi 1	0.99366	0.984347

k- $\epsilon$  turbulence model and compared the results to those obtained from an experimental setup show in figure 2.2.

Table 2.2: Results

Reading No.	Experiment	CFD analysis
1	0.9724	0.9619
2	0.9592	0.9689
3	0.9779	0.9692

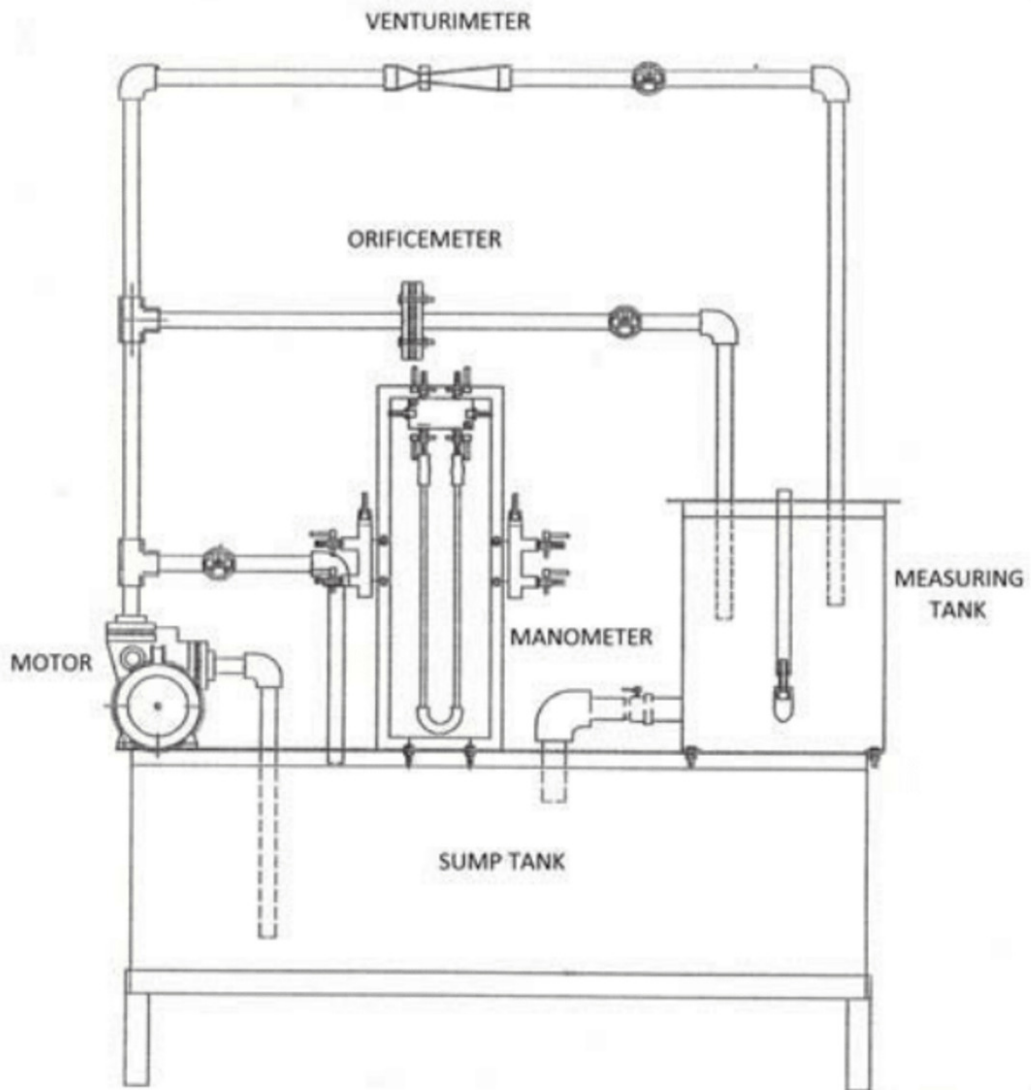


Figure 2.2: Experimental setup by Tamhankar et al [6]

Table 2.2 shows the results obtained from the study

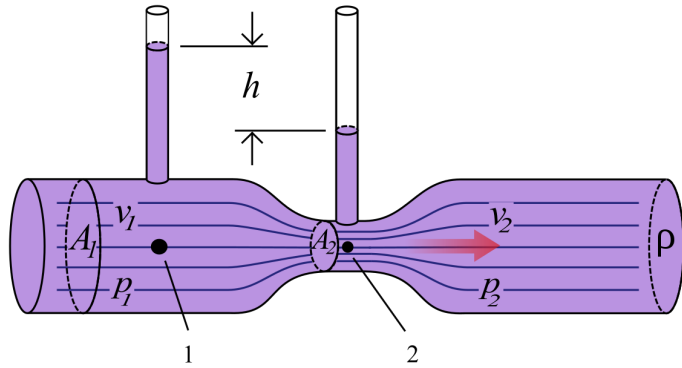


Figure 2.3: Venturi meter [7]

The study concluded that difference in values of the coefficient of discharge obtained from the model and those obtained from the experimental setup was less than 5% .

### 2.2.2 Analytical Predictions

This technique utilizes the Bernoulli's equation to establish an analytical correlation between the fluid flow and the coefficient of discharge of the Venturi meter.

Figure 2.3 shows the Venturi meter. Assuming the flow is ideal and applying the Bernoulli's equation before and after the contraction,

$$\frac{p_1}{\rho g} + \frac{v_1^2}{2g} + z_1 = \frac{p_2}{\rho g} + \frac{v_2^2}{2g} + z_2$$

But  $Z_1 = Z_2$ ,

$$\begin{aligned} \frac{(p_1 - p_2)}{\rho} &= \frac{(v_2^2 - v_1^2)}{2} \\ \frac{(p_1 - p_2)}{\rho} &= \frac{v_2^2}{2} \left(1 - \frac{A_2^2}{A_1^2}\right) \\ \frac{\Delta p}{\rho} &= \frac{v_2^2}{2} (1 - \beta^4) \\ v_2 &= \frac{1}{\sqrt{1 - \beta^4}} \sqrt{\frac{2\Delta p}{\rho}} \end{aligned} \tag{2.2}$$

Applying the continuity equation to the result of the derivation in 2.2,

$$\begin{aligned} Q_{th} &= A_1 v_1 = A_2 v_2 \\ Q_{th} &= A_2 v_2 = \frac{1}{\sqrt{1 - \beta^4}} \frac{\pi d^2}{4} \sqrt{\frac{2\Delta p}{\rho}} \end{aligned} \quad (2.3)$$

Equation 2.3 of theoretical flow rate is based on the assumption that the flow is steady, incompressible, inviscid, irrotational, no losses and the velocities  $V_1$  and  $V_2$  are constant across the cross section [8].

$$Q_{act} = \frac{C_{std}}{\sqrt{1 - \beta^4}} \frac{\pi d^2}{4} \sqrt{\frac{2\Delta p}{\rho}} \quad (2.4)$$

The frictional and viscous losses in a laminar flow can be estimated by the Darcy's law

$$H_L = \frac{(\Delta p)_{viscous}}{\rho g} = f \frac{v^2}{2g} \frac{D}{D} \quad (2.5)$$

where 'f' is the friction factor.

Coefficient of discharge equation 2.7 where for laminar flow, 'f' is given by equation 2.6 . This equation is derived from both the Darcy's law equation and the theoretical flow rate equation 2.3.

$$f = \frac{64}{R_{ed}} \quad (2.6)$$

$$C_d = 0.995 \sqrt{\frac{1}{(1 + 3f)}} \quad (2.7)$$

Arun et al [8] did a comparision of the  $C_d$  obtained by this method and that obtained

from a CFD simulation. The study concluded that the results from the two methods had an uncertainty of 0.9%.

## 2.3 Related Works

Discharge collection techniques have been developed for various applications. Some of these applications are related to the discharge collection unit used in the Synthetic Hydro-Experimental machine.

### 2.3.1 Electromagnetic activation

Angelo et al [9] implemented this technique in the design and testing of an Modular Automatic Water Sampler(MAWS). They designed MAWS and mounted them on unmanned marine vehicle with the aim of collecting water samples for scientific campaigns in front of polar tidewater glaciers. Their main design considerations was the response time of the stopper since the MAWS were operated under water and at the risk of damage by glaciers. The actuation unit of the sampler is shown in figure 2.4.

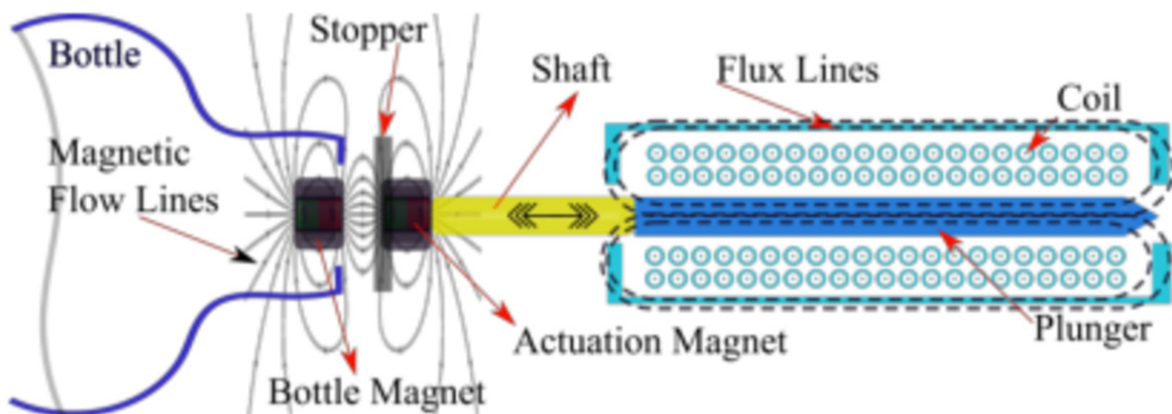


Figure 2.4: Sampler actuation mechanism [9]

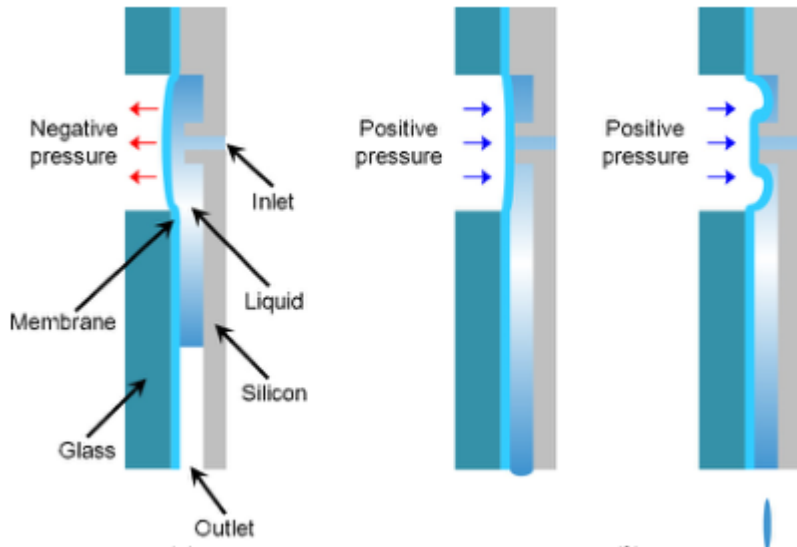


Figure 2.5: Dispensing mechanism [10]

When the coil in the solenoid is crossed by a current a strong magnetic field is generated that attracts the ferromagnetic plunger connected to the sealing stopper and opens the bottle allowing water to flow into the bottle's neck. As the current stops the two permanent magnets attract each other and the stopper seals the bottle [9].

### 2.3.2 Pneumatic Control

Pneumatic actuators utilizes the power of compressed air to impart motion on objects. Sangmin and Joonwon [10] did a design of cartridge-type pneumatic dispenser with a back flow stopper. The system used a membrane covering a discharge hole. The membrane was opened and closed using negative and positive pneumatic pressure respectively as shown in figure 2.5.

The application was able to do precise dispensation of 100nL to 400nL droplets.

## 2.4 Summary

Experiments involving the determination of the coefficient of discharge of the venturi or orifice have to include discharge and the measurement of some of its properties such as the time it took to collect, its temperature, and weight. In this literature, other techniques such as CFD and analytical methods have been found to be effective alternatives to using a hydraulics fluid test rig. These techniques have been proven to produce results with a difference of less than 1% from the experimental results obtained from a physical setup. Such results can also be obtained from the fluids rig currently used in JKUAT by automating the discharge collection unit. In this literature, discharge collection techniques that have proven to be effective in other applications and can be adapted for this automation have been covered. These techniques include the application of pneumatics and electromagnetism.

## 2.5 Gap analysis

1. The use of the CFD method undermines the credibility of the fluid flow experiments. This is because CFD mainly involves simulation. Furthermore, the technique is rather used for the design of fluid flow measuring devices.
2. CFD method can also be very resource intensive in terms of computing resources. Software used for this method requires a hefty license fee.
3. The application of the analytical method involves tedious calculations and several assumptions which can produce untrustworthy results.
4. The use of the Synthetic Hydro-Experimental machine with a manual discharge collection unit often produces results with huge error margins between 10-20 percent.

This project is entirely focused on addressing gap number four with the application of techniques such as pneumatics or electromagnetism. This closes in the technological gap

with the use of CFD, and simplifies the use of analytical methods by providing data for the computation of fluid flow properties.

## 3 Methodology

This chapter describes the design and fabrication of the three units that constitute this project.

- The discharge flow control unit
- The discharge handling unit
- the software and control unit.

### 3.1 Discharge Flow Control Unit

#### 3.1.1 Mechanical Design and Fabrication

This section describes the mechanical design and fabrication process for the flow control unit which consists of a servo motor holder, the LA-T8 linear actuator holder, a diversion flap, links, mounting straps, a valve interface, and motor mounting rods.

##### 1. Servo motor bracket

The servo motor bracket shown in figure 3.1 holds the motor in place and at the same time mounts the mounting rods in position through the mounting straps. The dimensions of the servo motor bracket are dependent on the dimensions of the MG996R servo motor. The slots on both sides of the bracket were to reduce the overall weight of the structure while the wedge was to offer extra support. The rectangular protrusion at the center of the bracket is meant to hold and fit the body of the MG996R servo motor which is 40mm by 19mm by 43mm hence the equivalent dimensions. The 1.50mm allowance on the width and 17mm height of the rectangular protrusion is meant to provide cooling to the motor while in operation. Finally, the overall length of the bracket (145mm) was guided by the length of the serrated straps keeping in mind that a single mounted rod is used to hold the two

pieces together. The two pieces thus had to be of the same length to perfectly fit. The bracket was designed with slots on both sides for manual realignment and fastening of the motor in position.

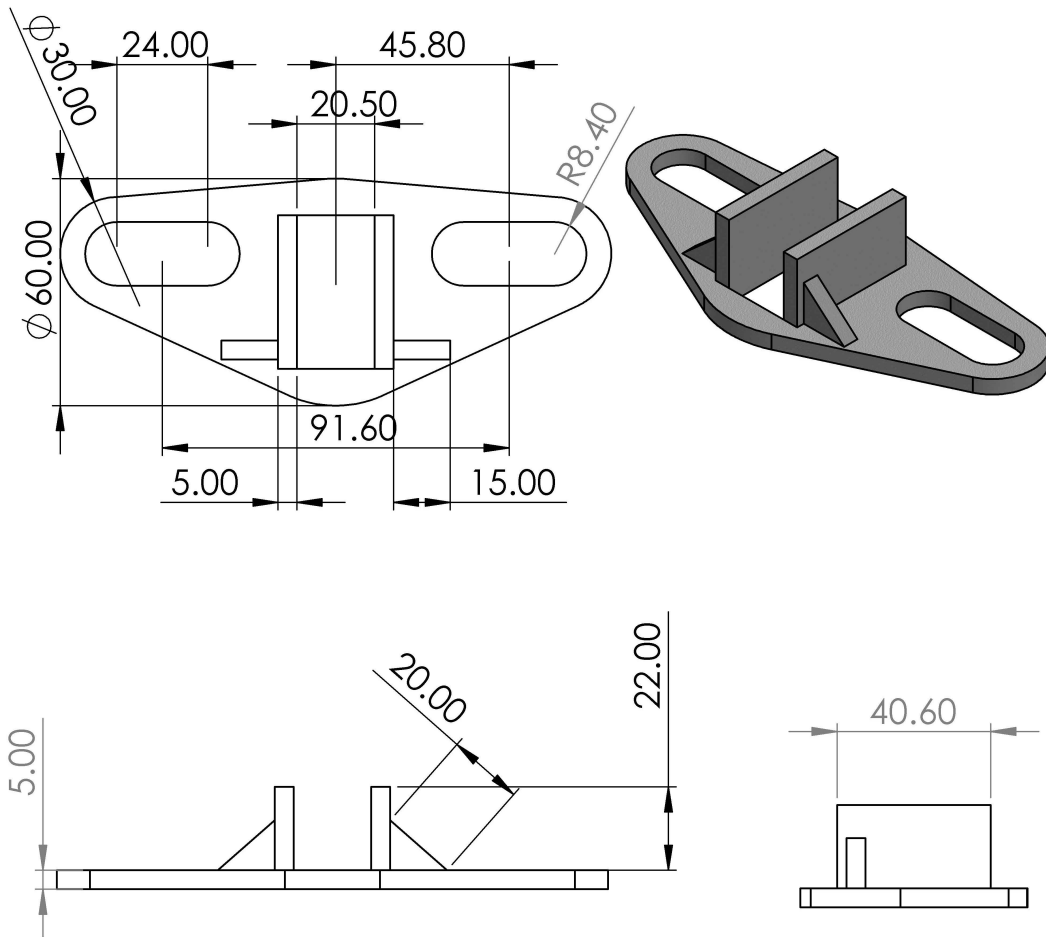


Figure 3.1: Servo motor bracket

The fabrication was done on an Ultimaker 3D printer. The process involved the conversion of the 3D CAD model into an STL file. The file was then sliced with a 40 percent infill and 0.15 mm layer height. The choice of these parameters was based on an estimation of the amount of twisting force this part would withstand on the test rig(1Nm). The printed servo motor holder is shown in figure 3.2.



Figure 3.2: 3D printed Servo Holder

## 2. LA-T8 holder

The LA-T8 holder holds the linear actuator in position. Figure 3.3 shows the design of the casing. The holder is mounted along the main discharge valve. It has to withstand the weight of the actuator and the diversion flap during operation. The overall dimensions as indicated in figure 3.3 of the LA-T8 holder were guided by the size of the actuator.

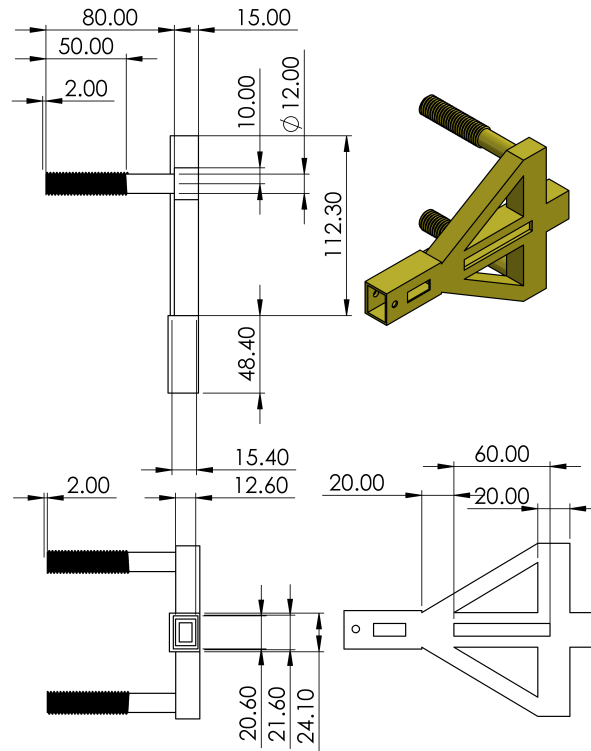


Figure 3.3: LA-T8 Holder

The width of 95mm is to enable it to be supported onto the ball valve on the

machine. The holder is mounted along the main discharge pipe supporting both the diversion flap and the flap support frame. The diameter was determined from the dimensions of the straps. An allowance of 0.5mm was provided to facilitate cooling when the actuator is in operation. Additionally, the slots on the side were to reduce the overall weight of the holder. The 0.5mm holes at the tip of the holder are to bolt the actuator with the holder in place to minimize on vibrations when in operation. Besides, being operated in a water-prone environment, the LA-T8 linear actuator had to be waterproofed from any splashes of the discharge hence the above design. The final 3D printed LA-T8 holder is shown in figure 3.4 below.

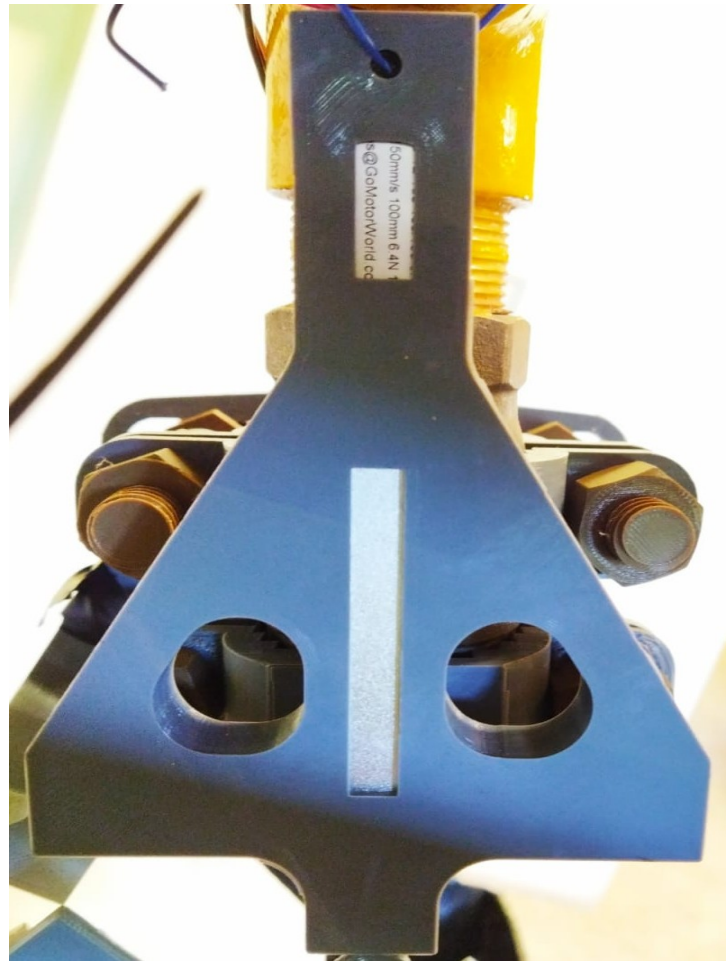


Figure 3.4: 3D printed LA-T8 holder

### 3. Straps

The serrated straps and mounting rods are used to hold the servo motor and the diversion flap in position. A total of four were used for this application. Two straps were used to hold the servo motor in place while the rest were used to mount the LA-T8 holder. Figure 3.5 and 3.6 show the 3D CAD designs of the top and bottom straps respectively.

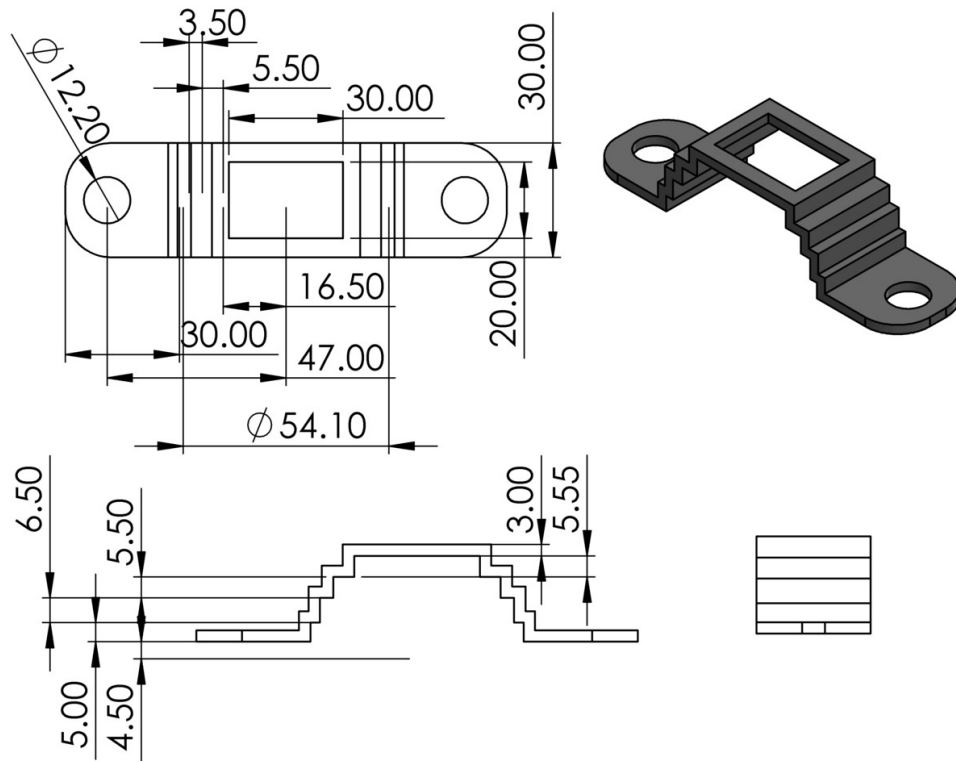


Figure 3.5: Top Strap

The overall dimensions of the top strap in figure 3.5 were a total length of 114mm with an internal diameter of 54mm. The strap is mounted on the existing ball valve casing on the machine with a diameter of 50mm hence the equivalent dimensions. The extra additional 4mm in diameter was to facilitate the ease of mounting the two straps together (top and bottom) to ensure that they firmly fit. The square pocket on the top strap was to allow for the mounting of the valve interface. The 30mm by 30mm dimensions were dependent on the protruding dimensions of the

existing ball valve casing. The serrations on the straps were to provide more grip while at the same time supporting more load.

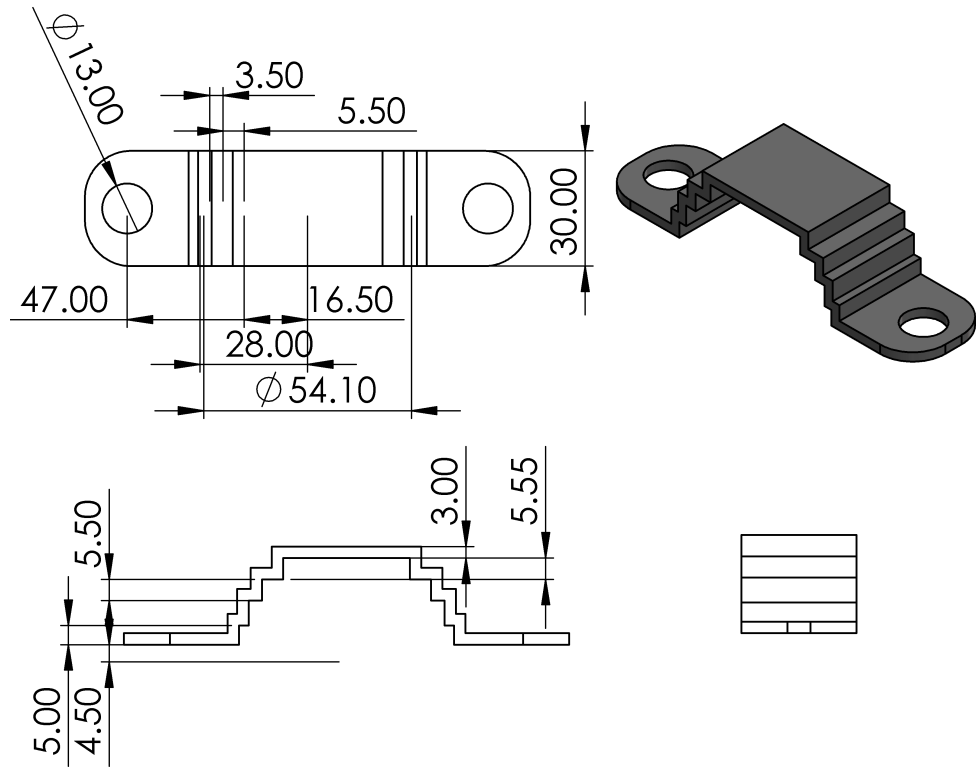


Figure 3.6: Bottom Strap

All the straps were 3D printed using the Ultimaker 3D printer. The above 3D CAD models were converted into STL files and sliced with the same settings as the servo motor bracket. Figure 3.7 below shows the printed parts.



Figure 3.7: 3D printed top and bottom straps

#### 4. Valve interface

The interface is used to connect the motor rotor to the ball valve to facilitate the actuation of the valve. Figure 3.8 below shows the interface design. It is fixed onto the motor using a nut while the other end is coupled to the motor shaft.

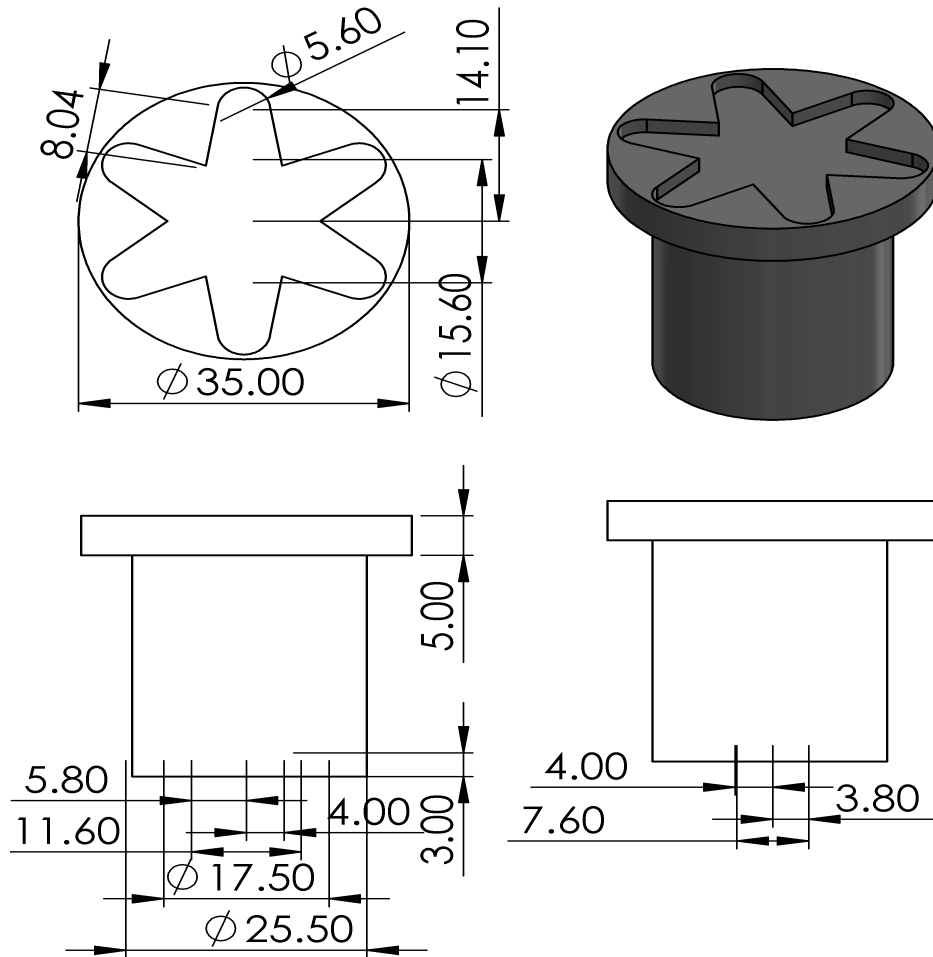


Figure 3.8: Interface

The dimensions of the interface such as the width of its base were measured directly and transferred from the existing ball valve. The overall height was dependent on the mounting rods hence the equivalent dimensions.

### 5. Diversion Flap

To divert the discharge, a channel-like flap is used. The design of the flap is shown in figure 3.9. The design was such that it can tap the whole stream from the  $1\frac{3}{4}$  inch main discharge pipe on the hydraulics test rig.

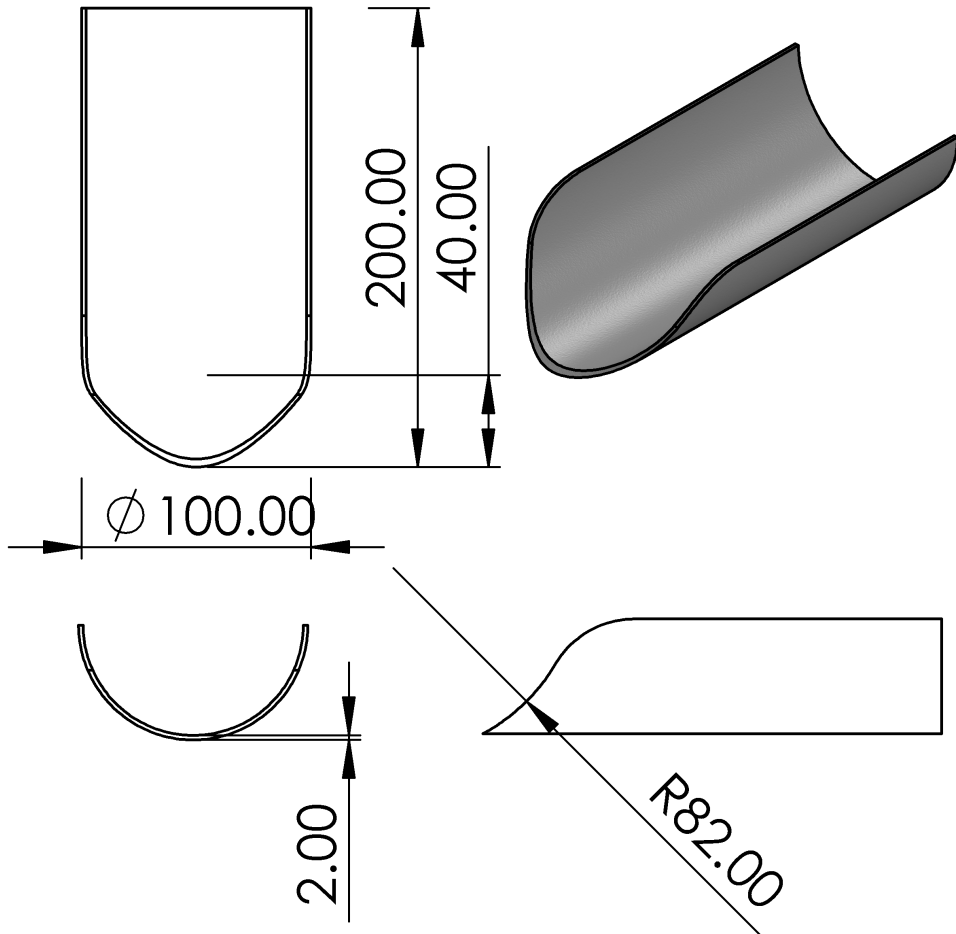


Figure 3.9: Diversion Flap

The flap was cut from a polyvinyl chloride (PVC) pipe as per the design dimensions. The 200mm length was determined by the length of the gap between the discharge pipe and the collection tank. It was necessary to ensure that there was free movement of the flap for proper diversion and no strain on the linear actuator. The dimensions of the selected PVC more so the width were guided by the diameter of the discharge pipe.

## 6. Mounting Rods

Two mounting rods are used to support the mounted servo motor assembly on the ball valve casing. The design of the rod is as shown in figure 3.10.

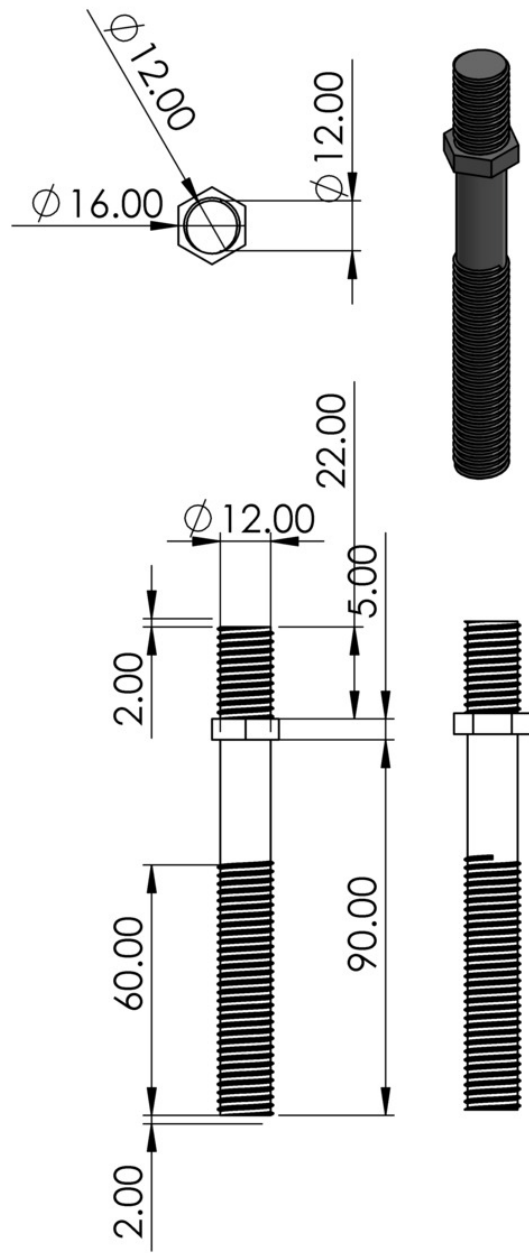


Figure 3.10: Mounting Rod

The choice to 3D print the mounting rods was the fact that the design allows for the fasteners on both sides; at one end to fasten the servo motor assembly after alignment and on the other end to fasten the whole flow control unit on the main

discharge flow pipe with the help of serrated straps. The protrusion on the surface eliminates the need for another fastener which would add to the overall complexity of the system. Figure 3.11 shows the 3D printed mounting rods.



Figure 3.11: Mounting Rod

### 3.1.2 Material selection

All the components from the servo motor holder, the LA-T8 linear actuator holder, a diversion flap, links, mounting straps, an interface, and mounting rods were all made from Polylactic acid (PLA). PLA was used due to its ease of use and minimal warping issues. The diversion flap is made from polyvinyl chloride (PVC). Furthermore, the use

of PLA and PVC served two main functions. The first was to eliminate the rusting of components that would have arisen with the use of metallic components. Secondly, was to cut down on the overall cost as it would not require preventive processes to prevent rusting.

### 3.1.3 Design Modifications

- **Link**

The link that serves to connect the linear actuator to the diversion flap was changed from that in figure 3.12 to that in figure 3.13 with the main modification being increasing the overall thickness of the link.

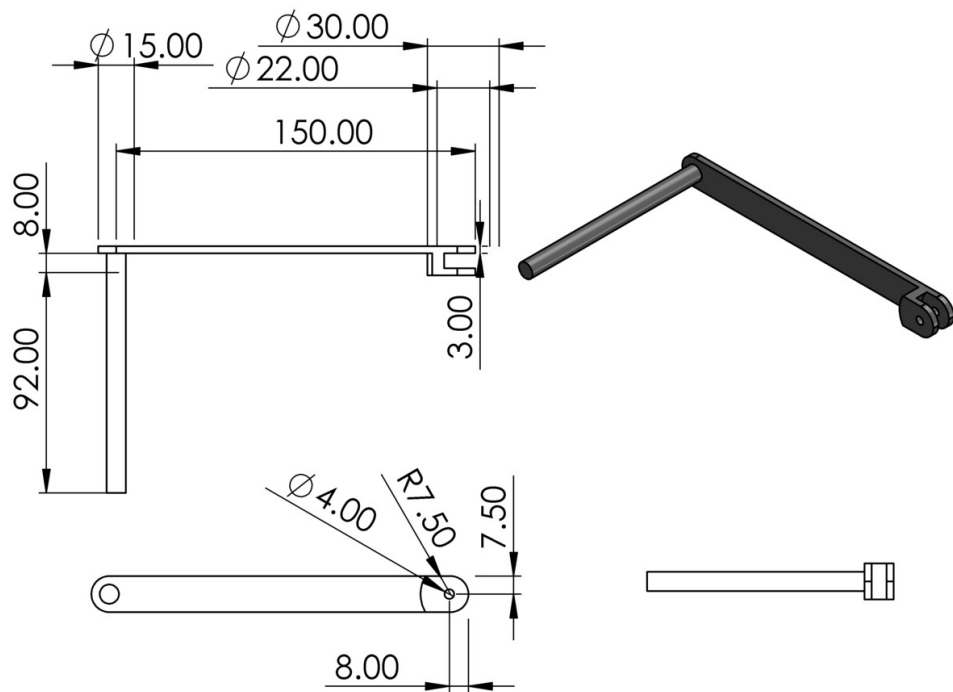


Figure 3.12: Link1

The thickness of the link was increased from 3mm to 5mm. This was because the initial link was warping under loading conditions when the flow was at its maximum pressure.

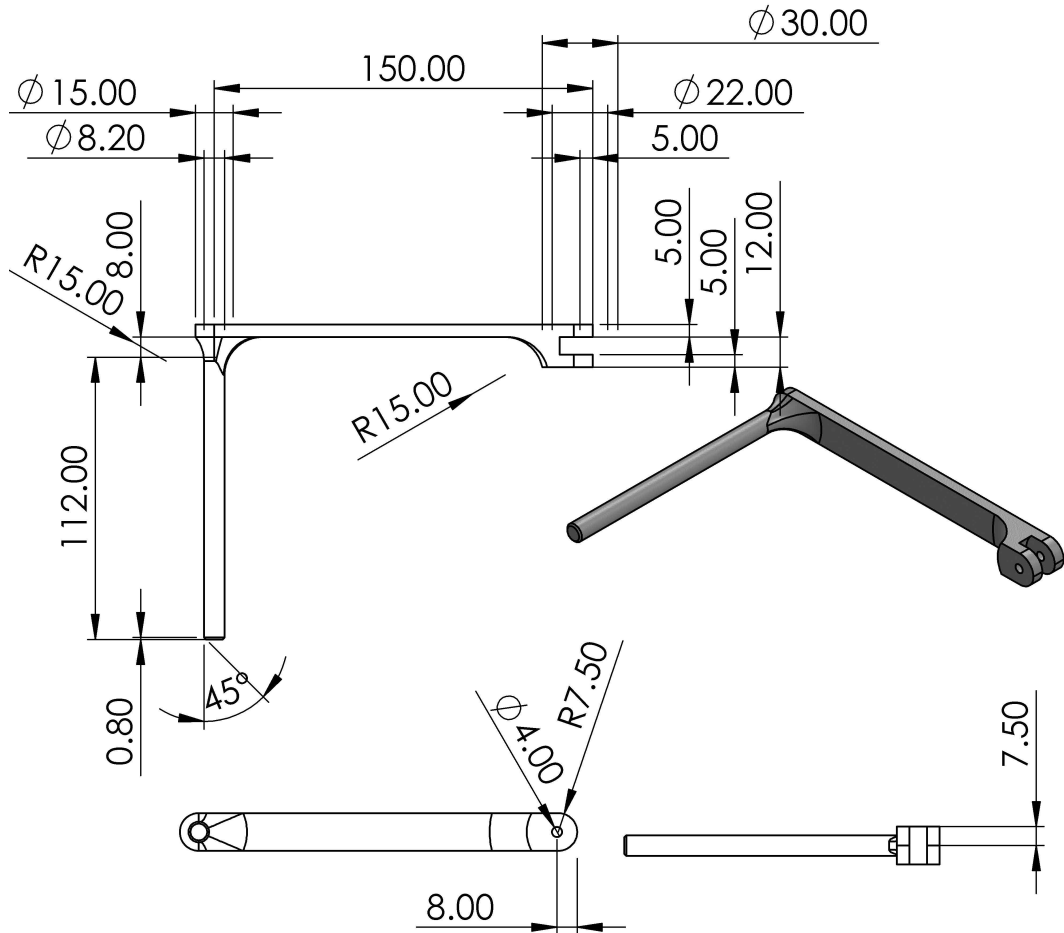


Figure 3.13: Link2

### 3.1.4 Electrical and Electronics

The discharge flow control unit has two electronic components. One is the MG996R servo motor used to control the flow rate in small precise steps. The other component is the L8-T8 linear actuator used for flow diversion.

- MG996R servo Motor

The MG996R servo motor was initially selected for turning the ball valve in precise steps. The motor is shown in Figure 3.14



Figure 3.14: 10Kg MG996R Servo Motor

The motor has the following features;

Table 3.1: MG996R Servo motor specifications [11]

Property	Value
Operating Voltage	+5V
Current	2.5A (6V)
Stall Torque	9.4 kg/cm (at 4.8V)
Maximum Stall Torque	11 kg/cm (6V)
Operating speed	0.17 s/60°
Gear Type	Metal
Rotation	0°-180°
Weight of motor and 55gm	

From table 3.1, the motor's power requirement includes an operating voltage of +5V. This means that any voltage above 5V may be hazardous to the motor while anything below may not power the motor. The motor's electrical circuit connection is as shown in figure 3.17. From figure 3.17 a buck converter is used to stepdown the 12V DC from the main supply to the rated 6V for the motor. The ground pin was grounded onto the STM32F407 microcontroller GND pin while the pulse width modulation(PWM) pin was connected to the pin PC8 of the same microcontroller.

There was however a change from the 10Kg MG996R servo motor to the DS8120

20Kg Metal Gear Digital Servo. This was because of a hinge inside the ball valve. The MG996R servo did not have enough torque to turn the valve past the hinge. Figure 3.15 shows the diagrammatic representation of the servo motor.



Figure 3.15: 20Kg Metal Gear Digital Servo

Table 3.2: MG996R Servo motor specifications [12]

Property	Value
Operating Voltage	4.8V-6.6AV
Current	2.5A (6V)
Stall Torque	18.5 kg/cm (at 4.8V)
Maximum Stall Torque	20.5A kg/cm (6V)
Operating speed	0.17 s/60°
Gear Type	Metal
Rotation	0°-180°
Weight of motor	60gm

The properties of the DS8120 are shown figure 3.2. It has similar external dimensions as the MG996R, this therefore did not necessitate any redesign in the motor bracket.

- **LA-T8 Electromagnet Actuator** The LA-T8 electromagnet linear actuator is used in tandem with the diversion flap to control flow diversion. The movement of the actuator coupled to the diversion flap via a link controls the flow of the discharge

either into the collection tank or into the main reservoir. The actuator is as shown in figure 3.16



Figure 3.16: LA-T8 Electromagnet Linear Actuator [13]

The actuator's technical specifications are shown in table 3.3.

Table 3.3: LA-T8 Micro-linear Actuator technical specifications [?]

Property	Value
Operating Voltage	6 or 12V
Stroke length	100mm
Stroke speed	150mm/s
Maximum Load	6.4N

The linear actuator is connected to a 4-pole relay controlled by the microcontroller for polarity switching. The relay is connected directly from the main 12V power supply. Figure 3.17 shows its electrical circuit connection.

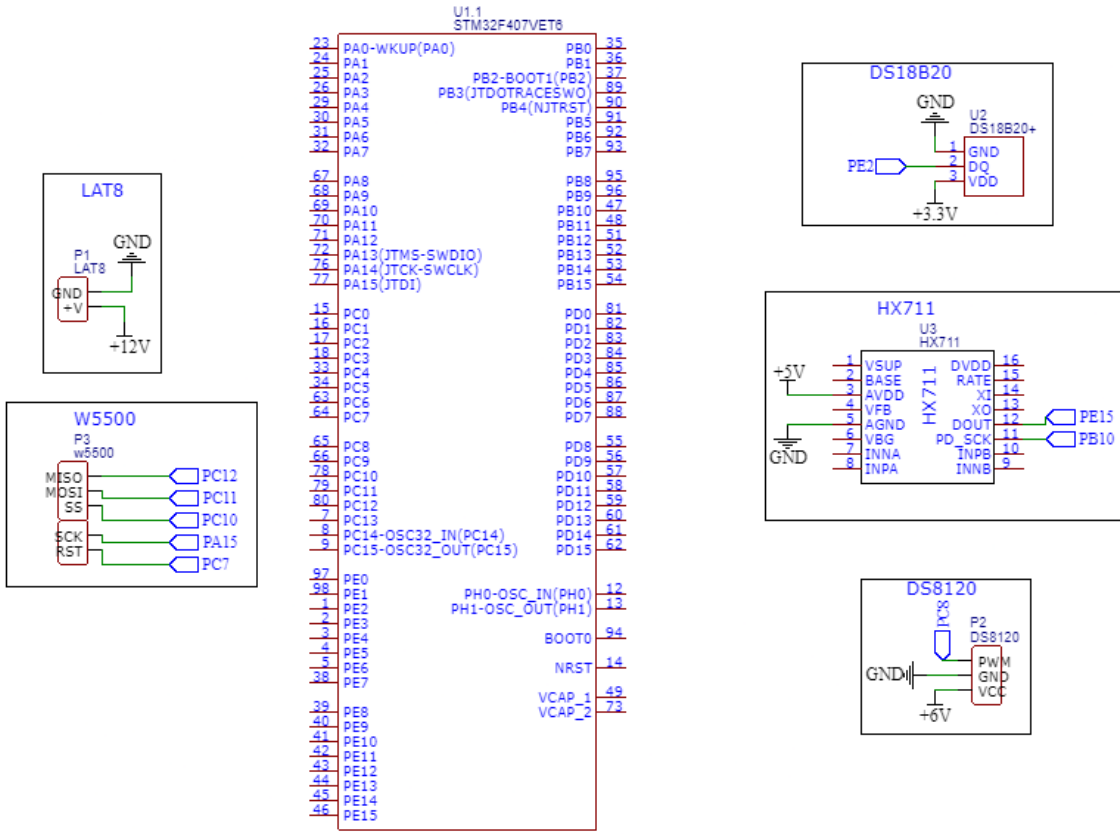


Figure 3.17: Electrical Circuit Schematic

## 3.2 Discharge handling unit

This unit collects the diverted discharge temporarily where its temperature and weight are taken. It consists of a discharge collection tank, an outlet valve, and weight and temperature measurement units.

### 3.2.1 Mechanical design and fabrication

#### 1. Discharge collection tank

The design of the tank was based on the following considerations:

- (a) The shape of the tank should be such that it induces the most discharge within the shortest time possible.
- (b) The tank should also be made of a material resistant to rust since it will be collecting chlorinated water.
- (c) The tank should also collect not less than 20 liters. This value is obtained from previous experiments on the rig.

From the above considerations, a horizontal cylindrical tank made of mild steel sheet was designed with dimensions shown in figure 3.18.

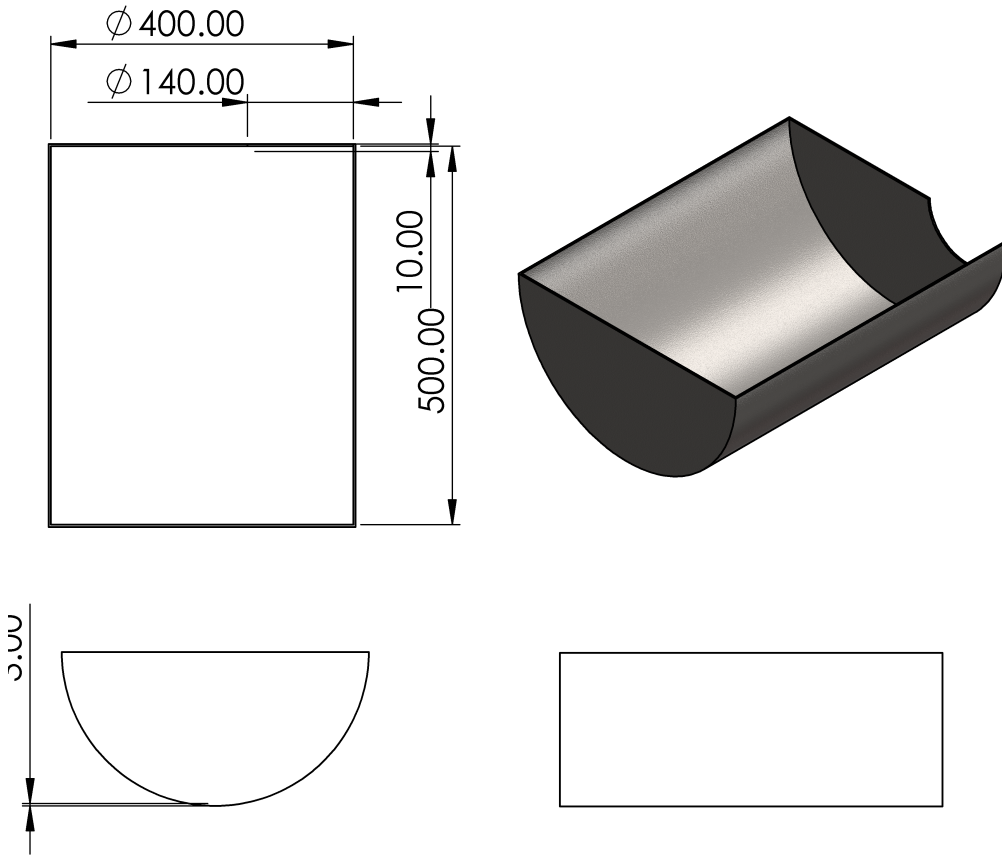


Figure 3.18: Horizontal Cylindrical tank

A support structure is necessary to support the tank. The design of the support frame is shown in figure 3.19 with its dimensions.

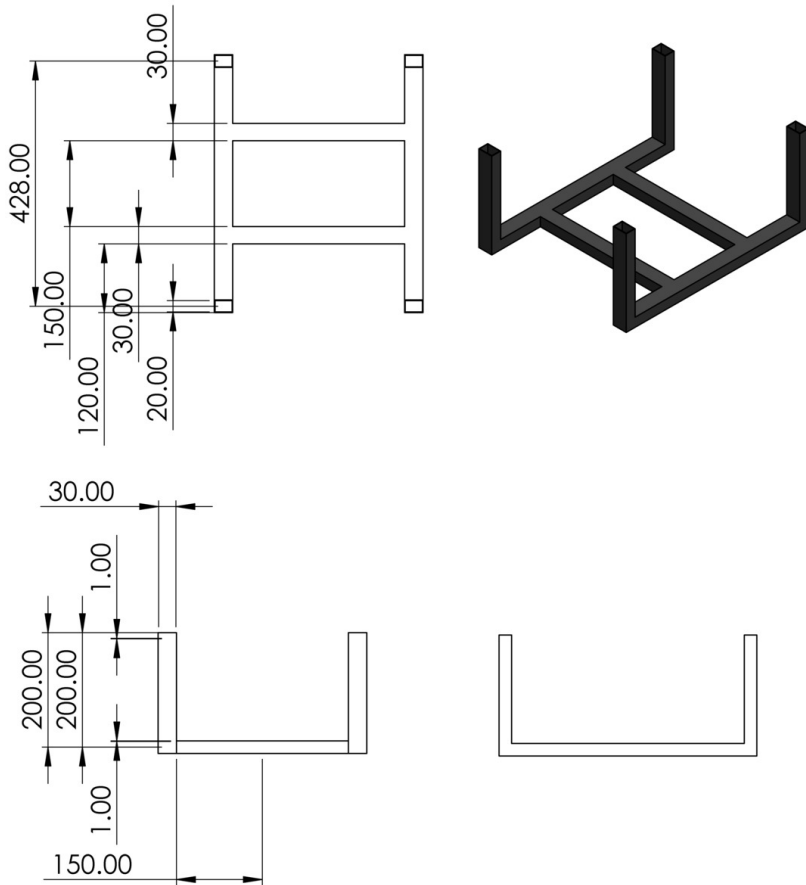


Figure 3.19: Cylindrical tank support frame

## 2. Fabrication

The fabrication of the tank started with the acquisition of  $2 \times 2$  meters of mild steel sheet. The dimensions of the sheet were obtained from the flattened sheet drawing of the tank. The sheet was then cut and rolled. The rolled sheets were welded together to produce the tank.

The tank was positioned in the center of the support frame, and welded as shown in figure 3.20. The assembly was painted to prevent it from rusting.

A  $1\frac{1}{2}$  inch ball valve was also welded to the bottom of the tank. This size of the valve was selected such that the tank could be emptied in the least time possible.



Figure 3.20: Fabricated tank

### 3. Tank support frame

A support frame is necessary to support the tank and the load cells on the fluids rig right under the discharge flow control unit. The selected design of the support is shown in figure 3.21.

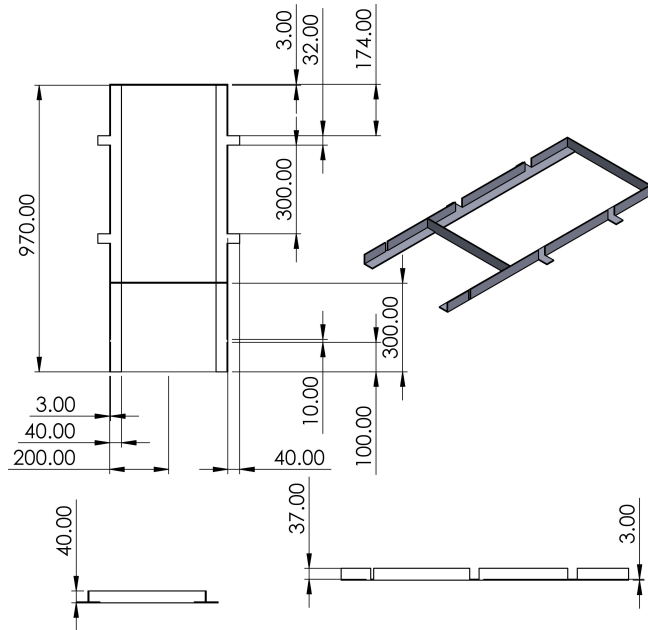


Figure 3.21: Tank support frame

The support frame was fabricated with  $40 \times 40\text{mm}$  angle lines. The angle lines were cut into the sizes from the design and welded together. It was later painted to prevent it from rusting. The extension flaps on the side were slit and hammered to flatten them. This provided support for the load cells.

#### 4. Cushion/suspension rubbers

For the selected load cells to perform efficiently, a pocket was made on the supporting surface to allow for the deflection of its resistive unit. Rough metallic support surface, could also provide unstable results. Therefore, a hard rubber cushion with a pocket shown in figure 3.22 was designed and cut.

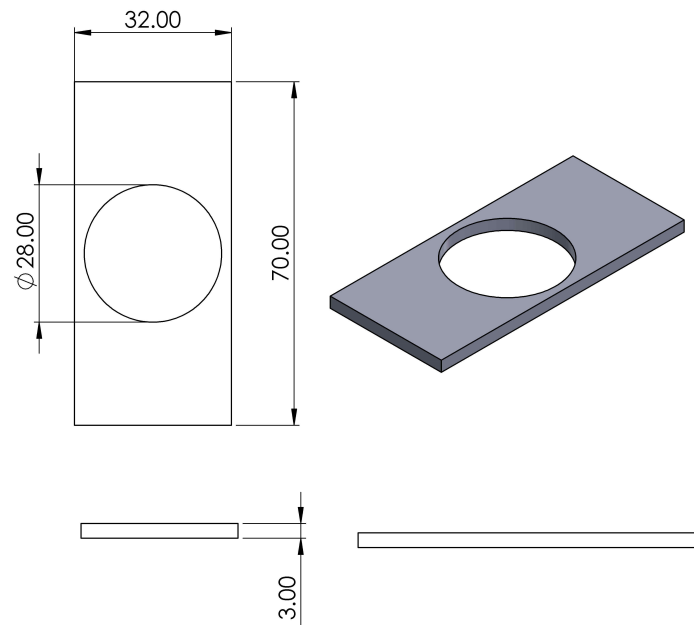


Figure 3.22: Cushion/suspension rubber

The rubbers are mounted between the load cells and the tank support frame as shown in figure 3.23.

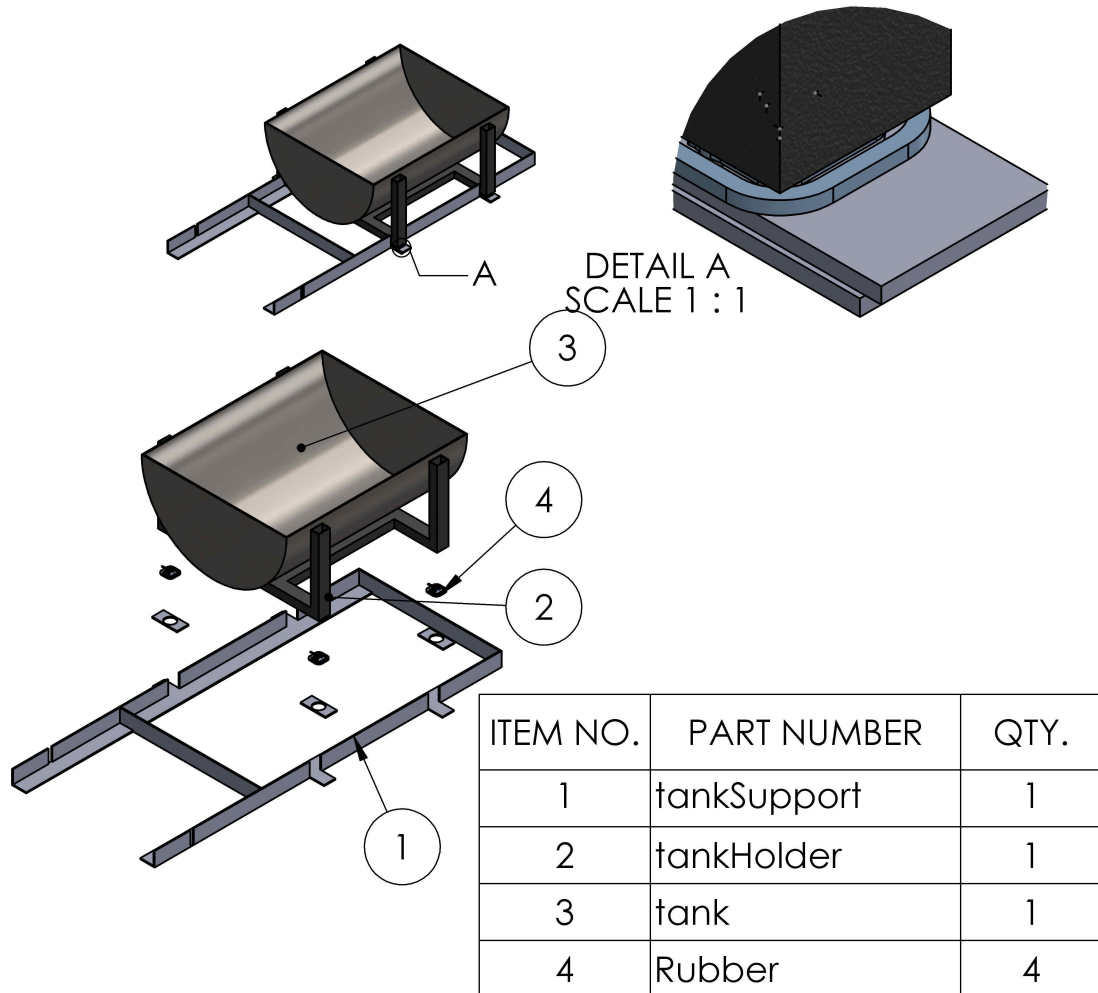


Figure 3.23: Mounted collection tank

##### 5. Plexiglass screen

A 400x400mm plexi-glass piece was also cut and fitted 100 mm from the edge of the support frame in order to minimize splashes of water during an experiment.

The assembly of these parts is shown in figure 3.24.

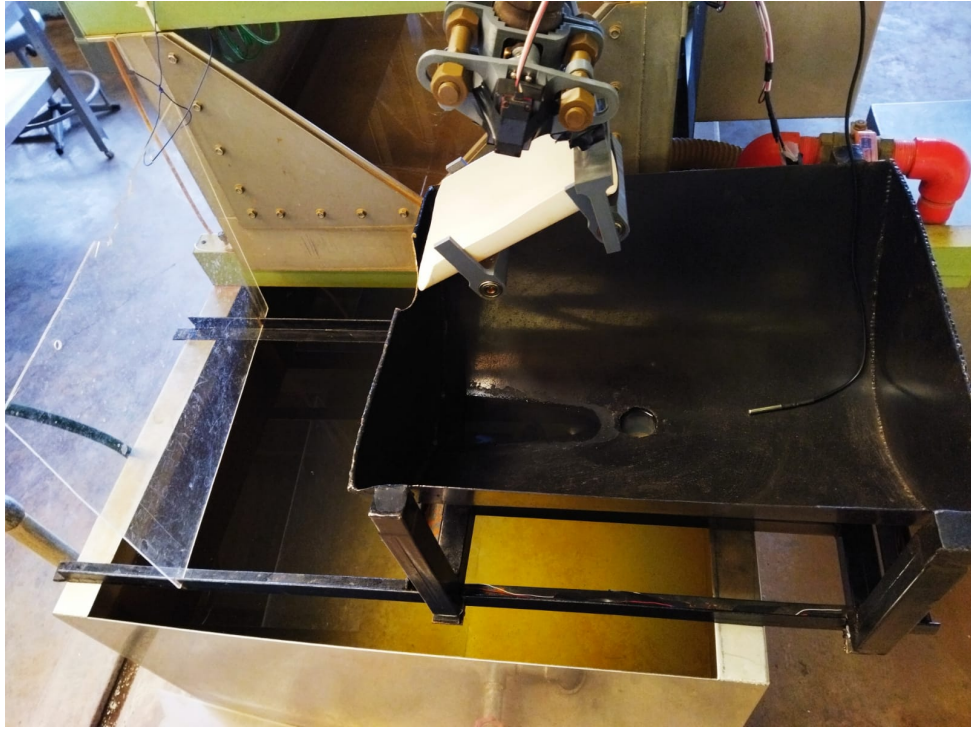


Figure 3.24: Fabricated discharge handling unit

### 3.2.2 Electrical and electronics

#### 1. Weight measurement unit

The weight of the discharge is measured in every run of the experiment. The selection of the weight measurement sub-unit was based on the following design consideration:

(a) The weight in the tank is distributed to the four vertices of the support frame.

This therefore necessitates four measuring units, each with a capacity not less than 20 kg.

(b) The resolution of the measuring device should be up to  $\frac{1}{100}$  of a kg.

Based on the above considerations, four load cells each with a range of 50 kg, one of which is shown in figure 3.25 were selected. They are distributed to the vertices of the tank as shown in the design in figure 3.26.



Figure 3.25: Strain-type load cells [14]

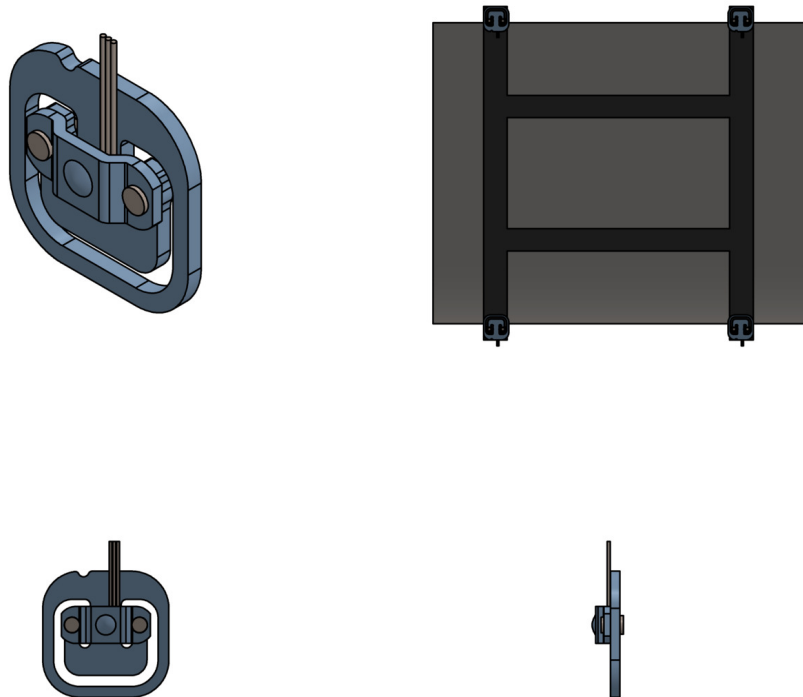


Figure 3.26: Collection tank with load cells

The four load cells are connected in a Wheatstone bridge as shown in figure 3.27.

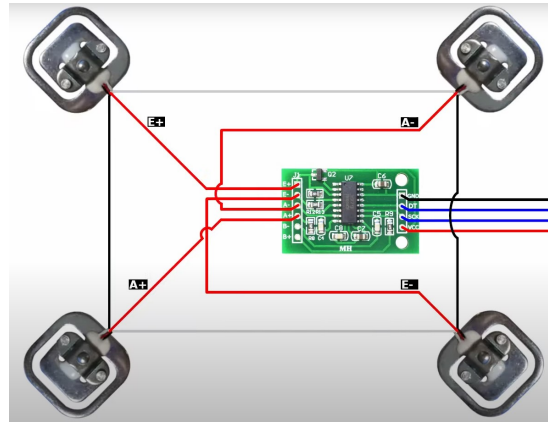


Figure 3.27: Load cell connection

The output of the load cells is amplified using an HX711 load amplifier which connects to an SPI interface of a microcontroller. The amplifier operates on a 5V DC supply which was provided by the microcontroller.

## 2. Temperature measurement sub-unit

The temperature of the discharge is measured at every run to ensure the consistency of the data collected. Since this measurement is taken within roughly 10 seconds before the outlet valve is opened, a measuring device whose sensitivity is enough to establish reliable results within that time is required for this application. An immersible DS18B20 temperature probe shown in figure 3.28 was selected. This probe operates on a 3.3V supply supplied by the microcontroller as shown in figure 3.17.



Figure 3.28: DS18B20 temperature probe [15]

### 3.3 Interface and control unit

This unit consists of two sub-units:

1. Interface and control sub-unit - which contains the graphical control of the system
2. Software and controller sub-unit - which contains the selected microcontroller for this application and firmware specifications for the application developed for the microcontroller.

#### 3.3.1 Interface and control sub-unit

It provides a means of interaction between the system and the user. Ideally, this sub-unit enables the user to input instructions and control the processes in this system. The status and results of processes in this system are also displayed in the interface. The choice of an interface depended on the following factors:

- **Interface choice considerations**

1. Size

This is the size of the operable part of the interface. In the case of a touch interface, a minimum of a 320x240 LCD is required to enable at least the minimum operability of GUI items, and a 20x4 LCD for any other choice.

2. Ergonomics

The user should be able to spend the least possible time feeding input and reading the results with relative ease.

3. Aesthetics

The interface will be mostly used by students with limited exposure hence good look might be motivating. However, this should not compromise the design. It should be able to be introduced and improved with minimum modifications to the hardware in the system.

A 320x240 touch LCD interface was selected for this application. This choice satisfies all the requirements required of an interface for this application. In addition, one can also add control or improve the aesthetics of the design by simply tweaking the GUI software without major hardware changes.

- **Interface Design**

The interface of this application was designed with the selected electronics in mind.

It included three screens:

1. **Home screen** - included all manual controls for the application.
2. **Screen 1** - included all automated controls for carrying out a coefficient of discharge experiment.
3. **Screen 2** - included controls for establishing wired control of the application from a remote personal computer(PC).

The mock designs for this application were made in Figma online designer. The designs were then implemented using LVGL, a lightweight graphics library for embedded systems. The library is designed to run only when deployed to embedded controllers. However, a simulator can be developed on a PC for testing. Figure 3.29 - 3.31 shows the developed interfaces for this application.

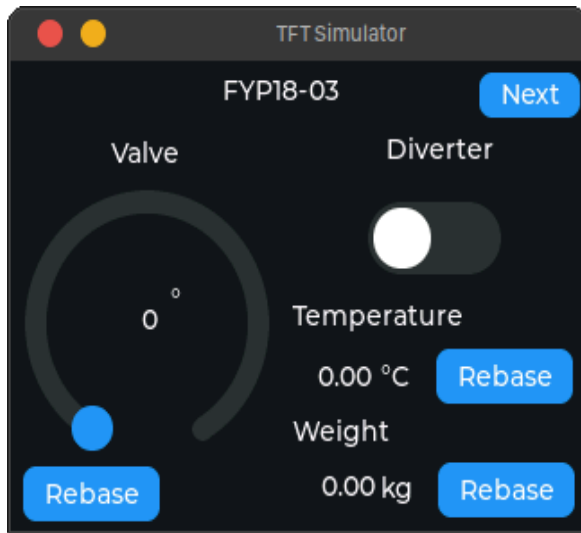


Figure 3.29: Home screen

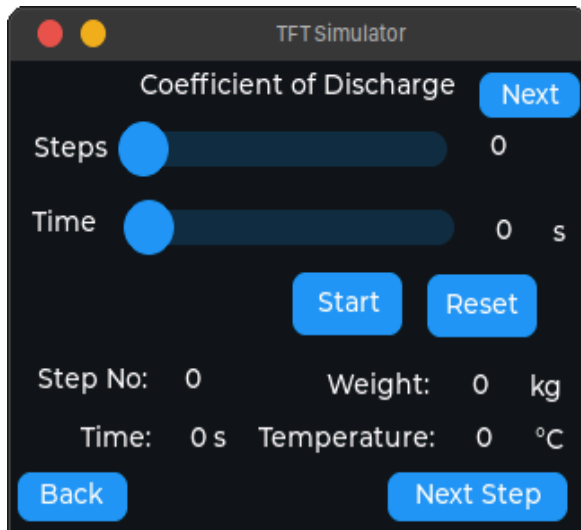


Figure 3.30: Screen 1

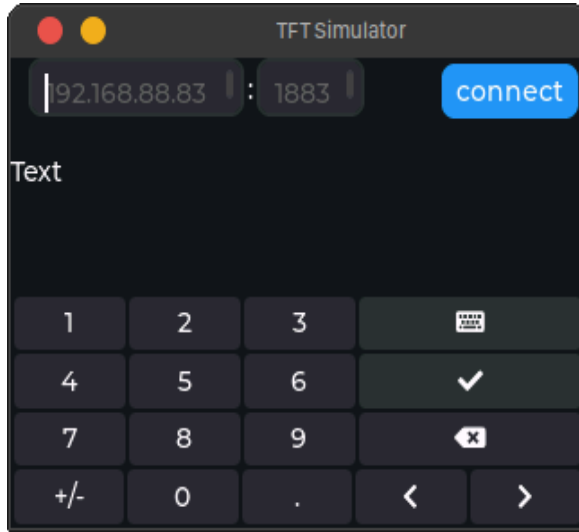


Figure 3.31: Screen 2

### 1. Home screen

The arc dial is provided for operating the valve through a servo motor in steps of  $1^{\circ}$ . A toggle switch is used to operate the linear actuator which in turn operates a flap that diverts a flow from the stream.

The temperature and weight readings are continuously updated in the temperature and weight labels respectively.

Rebase buttons are used to reset each operation.

### 2. Screen 1

Screen 1 provides horizontal sliders for setting the number of steps and the time interval for a coefficient of discharge experiment. Clicking the start button, the value of the time and step sliders are used to compute the distribution of the operating points of the servo and the linear actuator in order to complete the experiment.

The reset button resets the experiment and the controls.

### 3. Screen 2

Screen 2 provides two text fields for an IP address and the port of the connected PC. These inputs are keyed in using a virtual keyboard. The connect button

initiates the business logic of establishing a connection and communicating with the PC. The virtual keyboard auto-hides. This exposes a whole text field behind where the log for the transaction between the PC and the application is displayed.

- **Application logic**

The control flow of the system is shown in figure 3.32. This flow is triggered only when performing coefficient of discharge experiments. It starts when a user clicks the start button, the application then computes the control points for the valve and the diverter based on the values set for the time interval and the number of steps for the experiment. The system then turns the valve to the first control point and simultaneously initiates a timer and discharge collection. The elapsed time is continuously monitored and a different action is only taken when it elapses otherwise discharge collection continues. When the time elapses, the system stops the discharge collection and starts the temperature and weight measurement of the collected discharge. The results of the measurements are continuously updated on the graphical display.

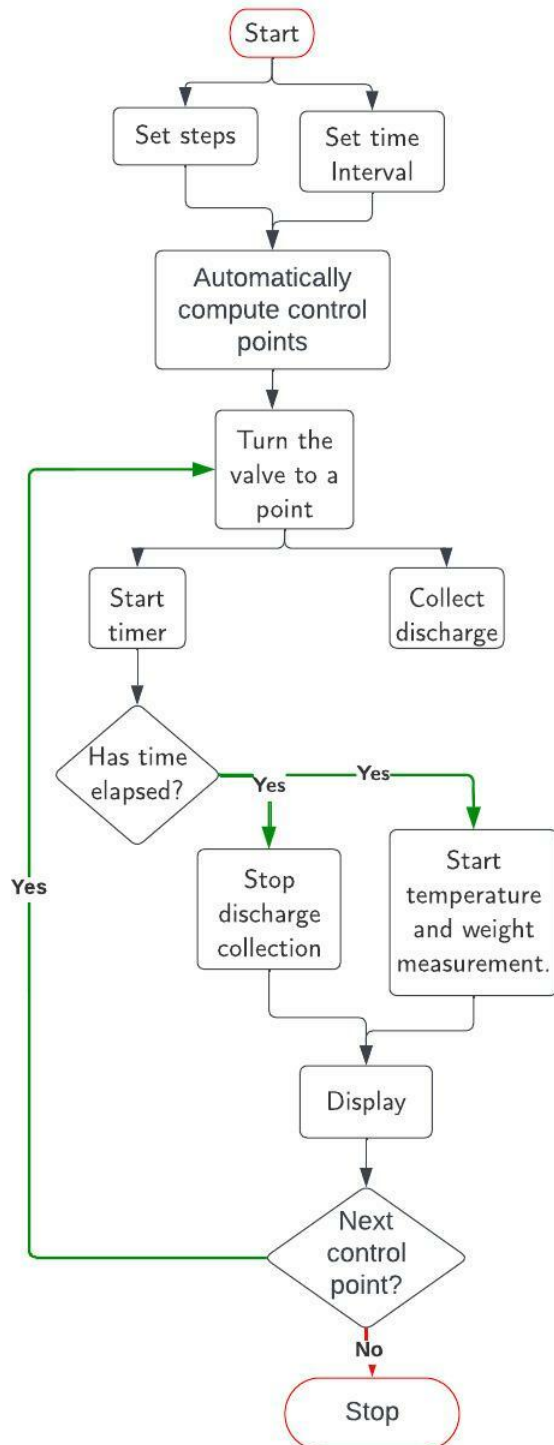


Figure 3.32: Application control flow

### 3.3.2 Software and controller sub-unit

This sub-unit executes the application logic, sends instructions to the actuators, and reads inputs from sensors in the system. It is responsible for synchronizing the GUI with the processes in the hardware. Besides, it monitors and controls the parameters of the input devices and generates output signals to implement desired tasks.

The selection of a micro-controller for this application was based on the following requirements:

1. Support for a touch LCD screen. 32 Digital I/O pins are required in order to support a parallel 16-bit MCU Interface, and a 16-bit data bus is required for this application.
2. Support for real-time multi-threaded firmware. This necessitates support from RTOS-operating systems. This is to allow for several threads, at least 2 threads minimum: one for handling the GUI, and another for handling the application's business logic.

A STM32F407VET6 microcontroller board shown in figure 3.34 was selected for this application. It has a dedicated FSMC interface for supporting LCD touch screens. Besides, it can also support real-time multi-threaded firmware.

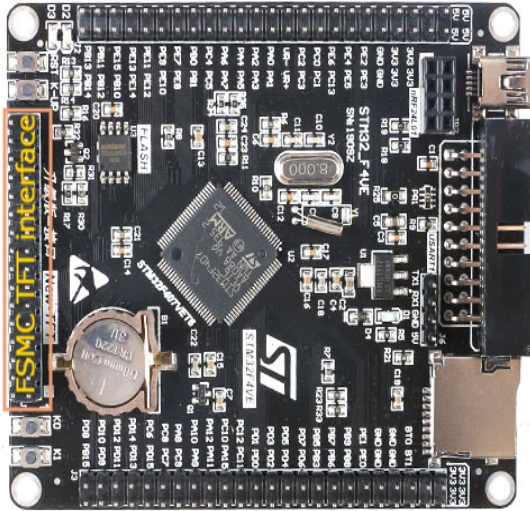


Figure 3.33: FSMC interface in STM32F407VET6 [16]



Figure 3.34: STM32 connected with LCD [16]

Mbed-OS RTOS was selected for the development of the firmware for this application. It has a vast amount of APIs that simplify development and abstract the HAL code.

- **Application architecture**

Figure 3.35 shows the architecture of the firmware for this application.

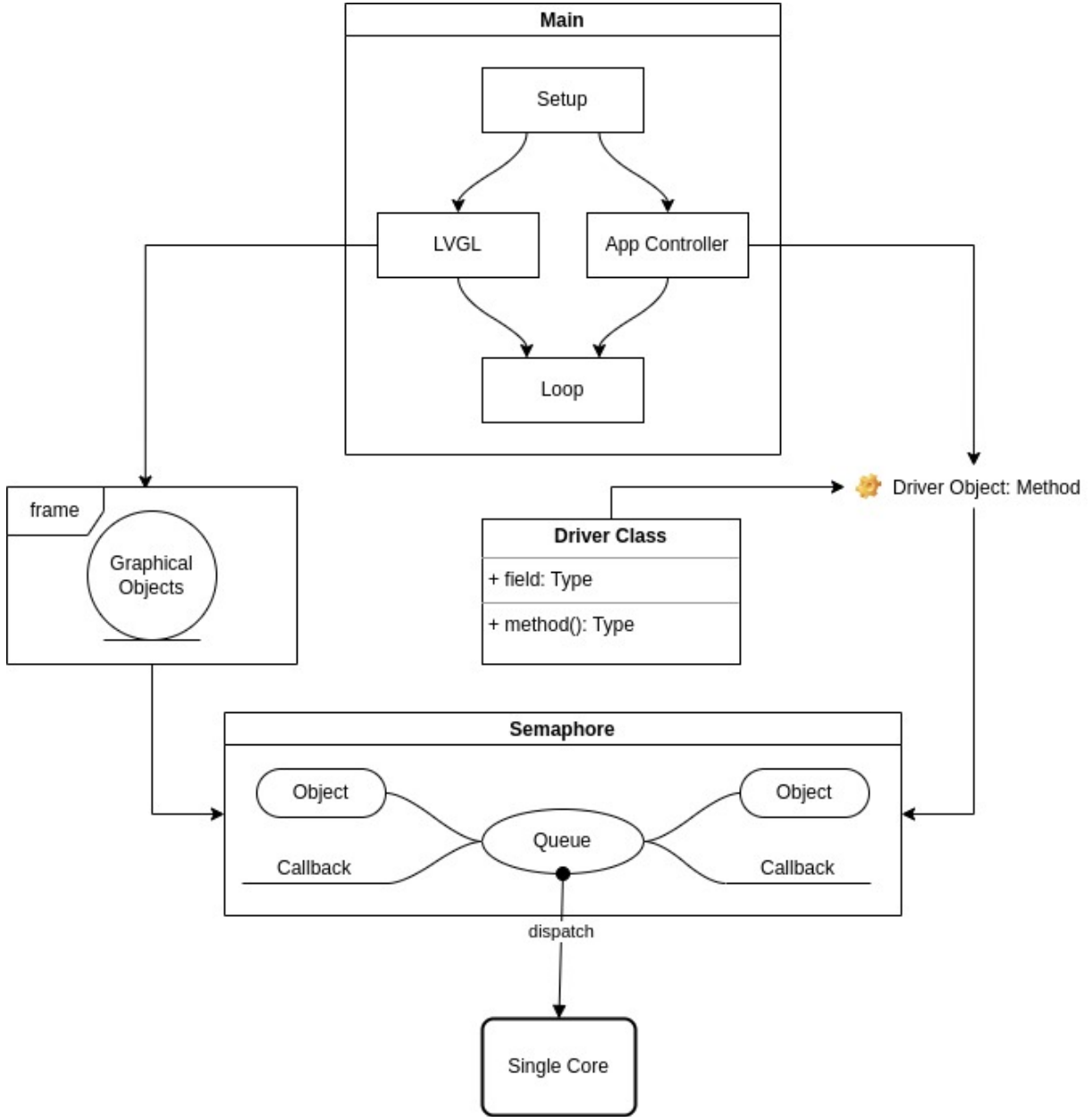


Figure 3.35: Firmware architecture

The application starts in the main function where time tickers have been created for updating the UI. A low-priority thread was created for handling the GUI, basically updating and refreshing the GUI elements every 200ms. Another above-normal priority thread is also created with an event queue for handling the business logic of

the application. This thread is controlled by an app controller class, which takes in the objects, functions, and function arguments of the driver classes and dispatches this into an event queue as events. Once an event has been dispatched, it can be canceled but it is unsafe as might lead to a memory leak.

The graphical objects have callbacks assigned to only certain events they might generate. Such callbacks communicate with the app controller thread using a semaphore and dispatch an event into the queue. This is handled by the single core on the microcontroller board.

- **Wired Remote Control**

The firmware for this application also supports remote control over an ethernet cable. This is enabled by a W5500 ethernet module onboard the electronics board. This type of control is also enabled by a desktop application shown in figure 3.36 made specifically for this application. The communication between the PC, and the microcontroller board is through a protobuf protocol with typed fields.

The setup for this type of control starts with setting a static IP address in a PC and then connecting the PC to the W5500 ethernet module, onboard the system. The same PC's static IP address is also inserted in the IP text fields on screen 2 of the application. The port is kept at 1883. The connection is established once the connect button is clicked.

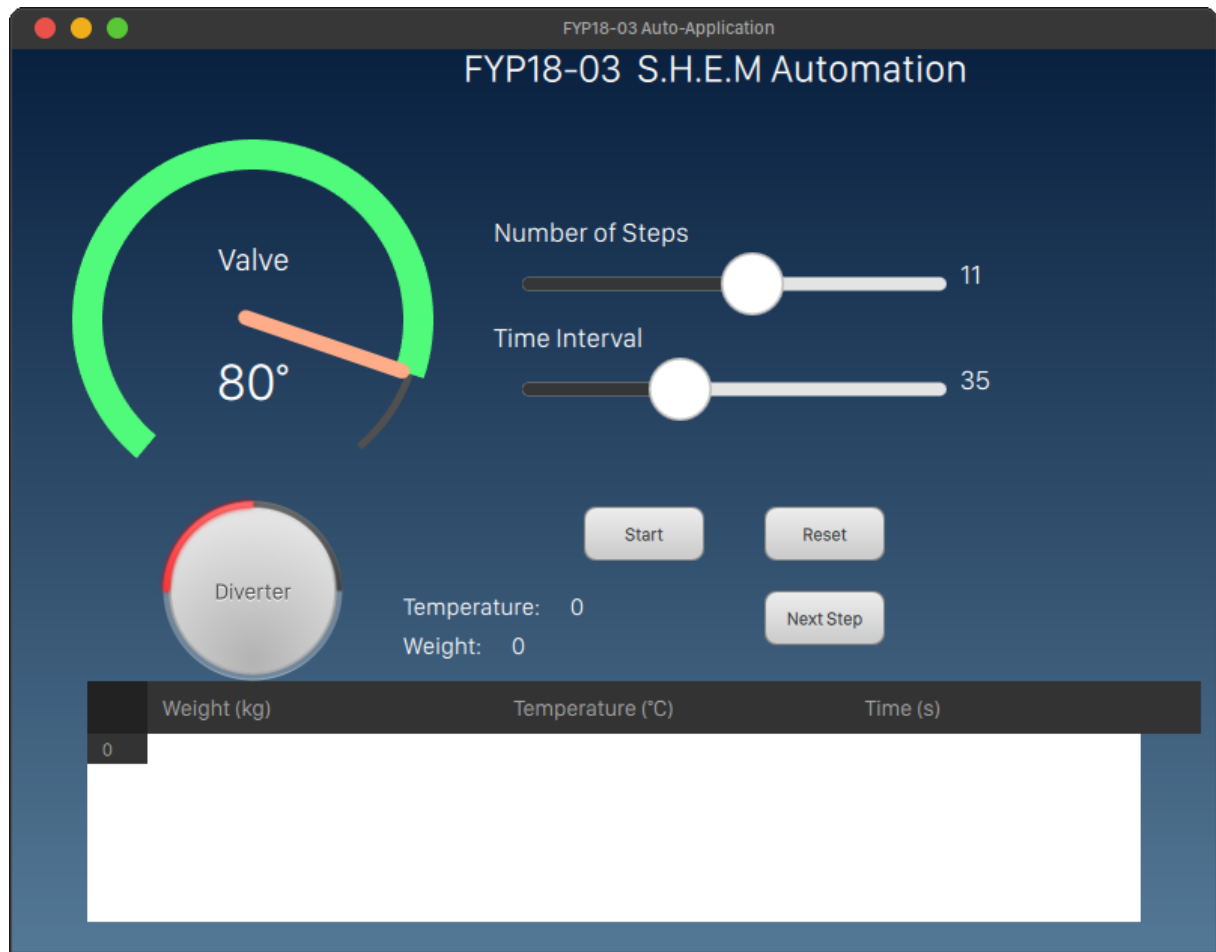


Figure 3.36: Desktop application

## 4 Results and Discussion

This section describes the results obtained from the three main sections of this project.

### 4.1 Final Design

The complete design in exploded view is shown in figure 4.1.

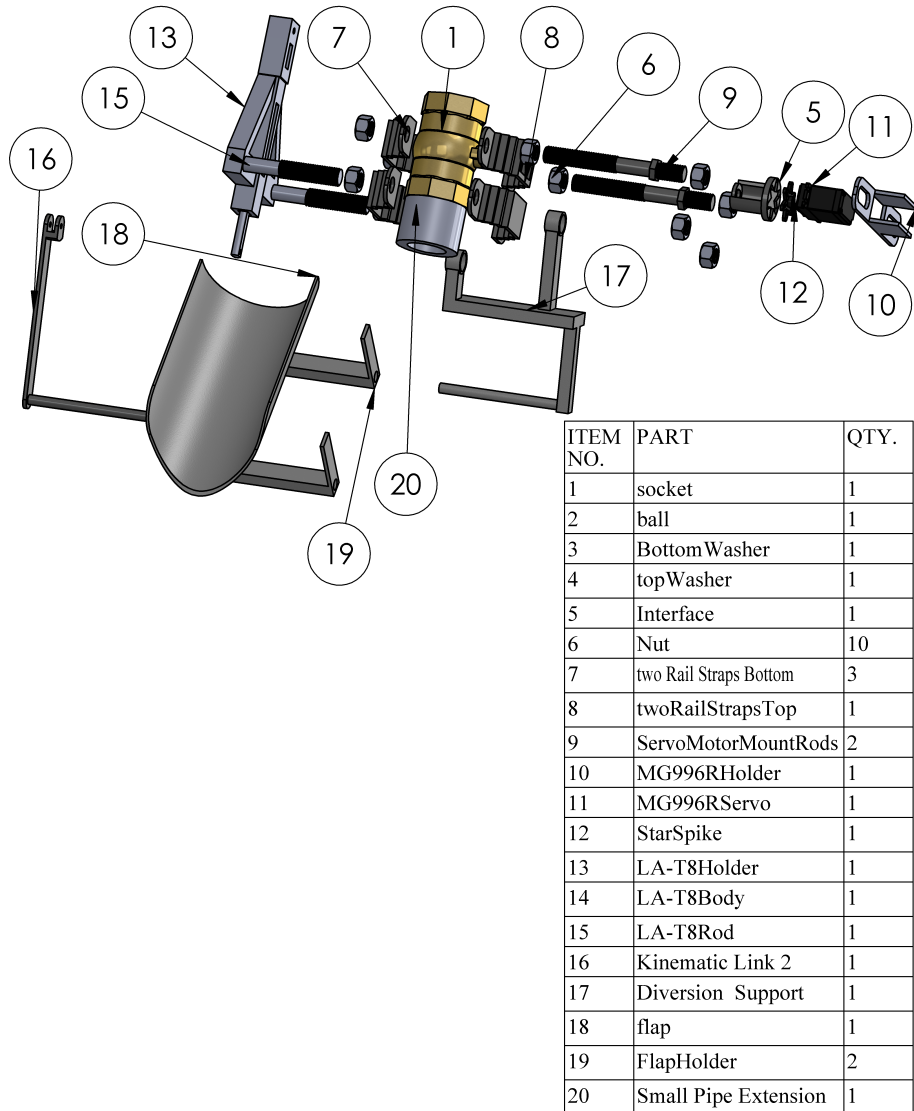


Figure 4.1: Unit Exploded view

## 4.2 The Discharge Flow Control unit

The objective of this unit was to design and fabricate an automated flow control mechanism that can operate the ball valve in steps of less than 1 degree and a flow diverter mechanism that can divert the flow in a second.

Figure 4.2 shows the virtual arc dial labelled 'Valve' that is used for opening and closing the ball valve. The dial has been programmed to operate the servo motor in steps of 1 degree.



Figure 4.2: Controls for the flow control

The protrusion on the ball valve, marking the closed position of the valve lever was used as a datum for testing and calibration. A full rotation from one face of the protrusion to the other about the center of the ball valve is equal to a 90-degree rotation. The selected servo motor covers this in just only a 76-degree rotation. This is a clear indication that the selected servo motor can turn in steps of less than 1 degree.

The LAT8 linear actuator used for flow diversion could divert the flow in between 1 second and 1.5 seconds depending on the pressure set in the main pump. Pressure equivalent to a barometric height of 390 mm across the venturi was found to be ideal for diversion in 1.2 seconds.

Figure 4.3 shows the assembly of the fabricated unit.



Figure 4.3: Discharge Flow Control Unit

### 4.3 The discharge handling unit

The objective was to automate weight and temperature measurements, and re-design the discharge collection tank such that it can discharge in the least time possible.

A DS18B20 temperature probe and four load cells were used for measuring temperature, and the weight of the collected discharge after every 200 ms. These values are continuously displayed on the interface.

The tank could also collect 25 kg of discharge, and is fitted with a  $1\frac{1}{2}$ inch ball valve at the bottom that can discharge a full tank in 12.73 seconds.

Figure 4.4 below, shows the assembly of the fabricated unit.

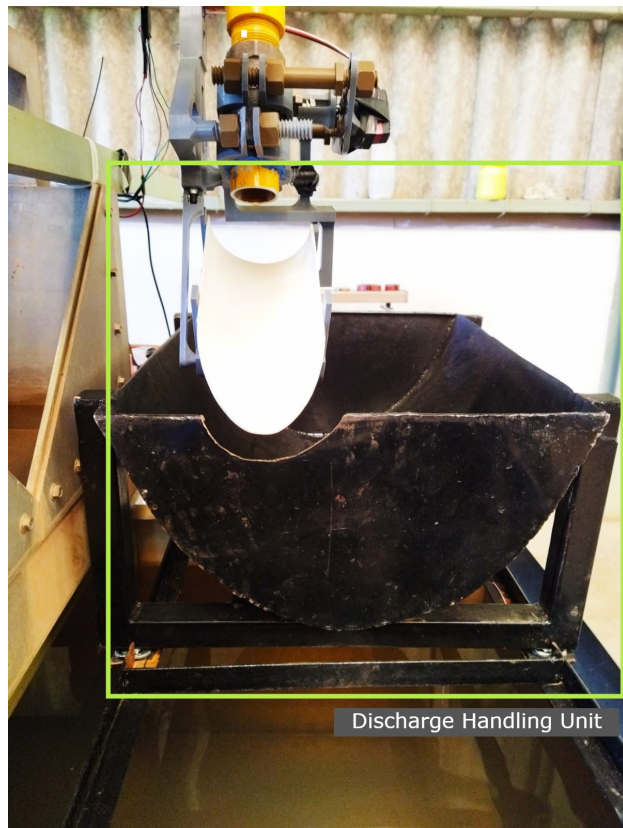


Figure 4.4: Discharge Handling Unit

#### 4.4 Electrical and Electronics Unit

Figure 4.5 and 4.6 show the electrical and electronic components developed on a protoboard including the components for the servo motor control, an LA-T8 electromagnet linear actuator control, an HX711, and a DS18B20 temperature probe.

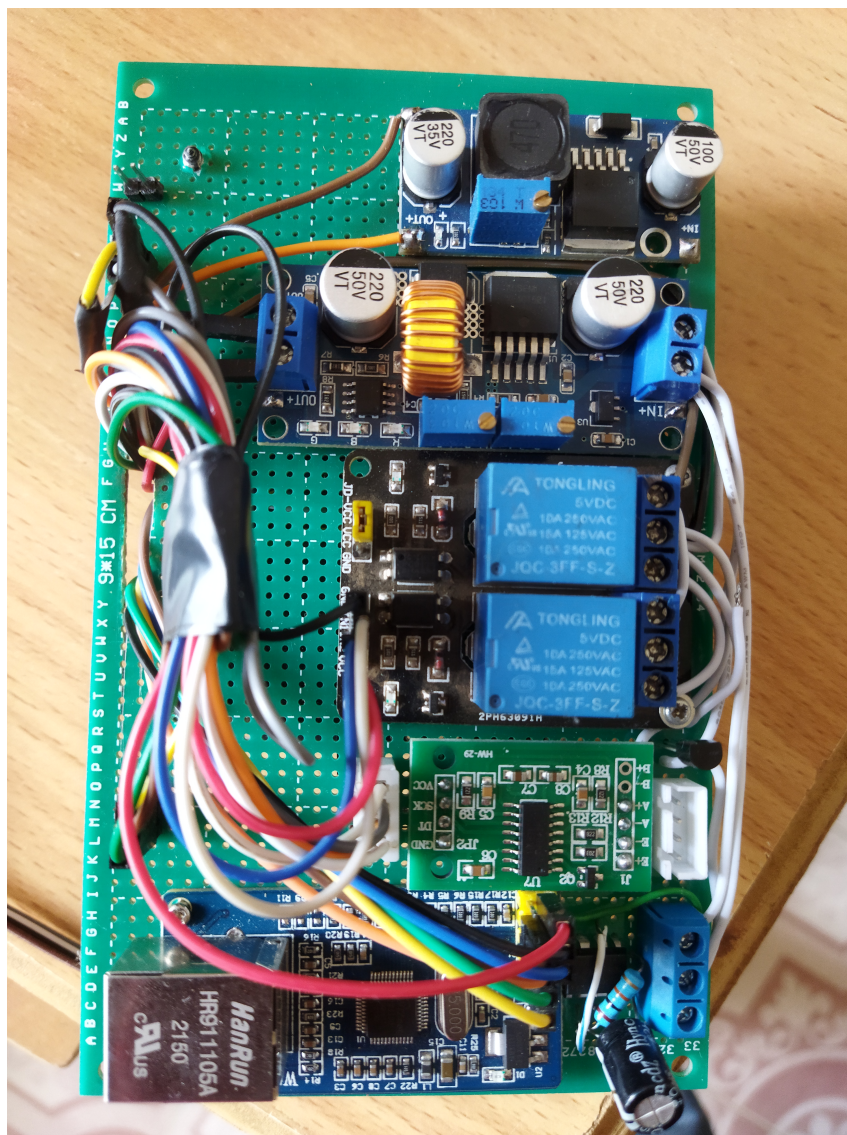


Figure 4.5: Electrical Assembly

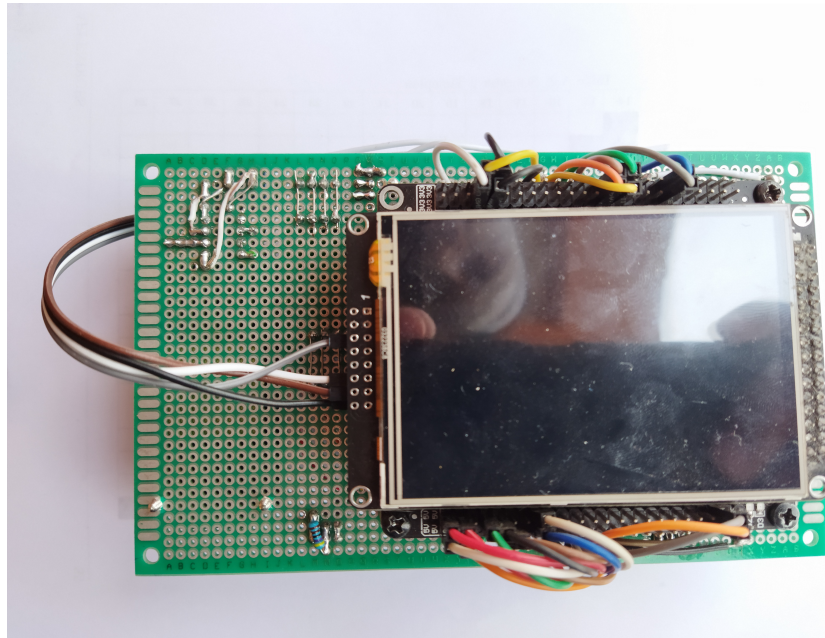


Figure 4.6: User Interface Mounted

## 4.5 Final Assembly

Figure 4.7 below shows the final assembly inclusive of the discharge flow control unit, discharge handling unit, and the interface and control unit. The unit is designed and fabricated as a plug-and-play, in that it is not permanently fixed onto the machine but can be removed to allow for other experiments to be conducted.

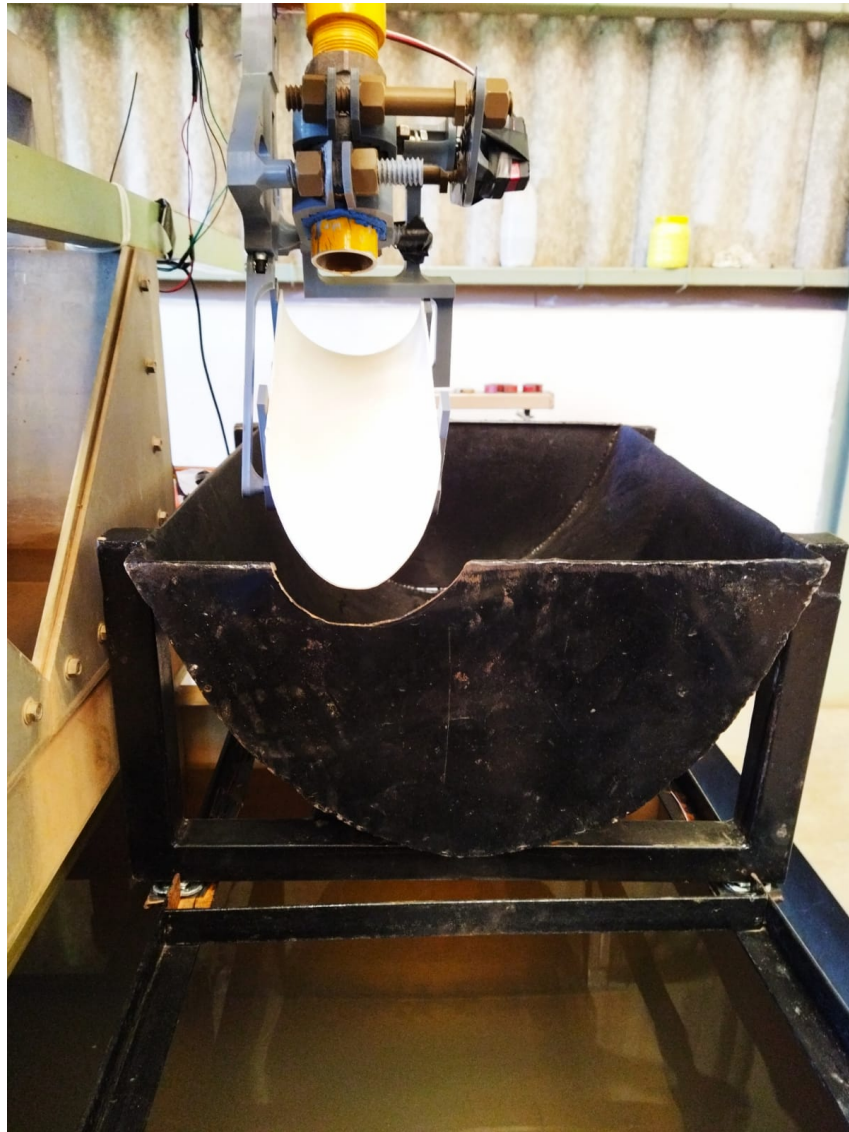


Figure 4.7: Finally Assembly

## 4.6 Experiments Conducted

The coefficient of discharge experiments was conducted using the system. The objective was to determine the coefficient of discharge from the system and compare it with the one obtained from manually conducting the experiment. This was so as to determine whether the system reduced the human error that resulted from the manual operation of the test

rig.

During the experiment, four runs were conducted in total. One involved manual operation while three were done with the automated system. With the system in place, it first reduced the number of operators from three to two. Secondly, when conducting the experiment, the user is required to only set the number of steps (runs) to perform the experiment and the maximum time interval. The system then auto-calibrates itself to determine the time allocation for each run. The results from each run are recorded via the necessary components and the values sent to be recorded under time, temperature, and weight.

#### 4.6.1 Experiment 1

Table 4.1 below shows the results obtained from the manual operation to determine the coefficient of discharge of the venturi.

Table 4.1: Manual Experiment

Step	Height 1	Height 2	Head	Weight 1	Weight 2	Weight	Temperature	Time
0	0	0	0	0	0	0	0	0
1	665	657	8	22	27.4	5.4	21	50.51
2	657	642	15	27.4	36.1	8.7	21	42.56
3	647	613	34	36.1	40.9	4.8	21	30.3
4	623	514	109	40.9	58.1	17.2	22	21.74
5	594	428	166	58.1	67.7	9.6	22	18.44
6	562	317	245	67.7	81.1	13.4	22	15.39
7	548	282	266	81.1	93.7	12.6	22	12.53
8	522	212	310	93.7	103.6	9.89999999999999	22	8.05
9	500	153	347	106.6	111.5	4.90000000000001	22	5.13
10	474	85	389	111.5	115.3	3.8	22	3.6

From table 4.1, a graph of the actual flow rate ( $Q_{act}$ ) versus the square root of the differential  $(h_1 - h_2)^{1/2}$  head was plotted as shown in Figure 4.8. The coefficient of discharge  $C_d$  was found to be 0.747773.

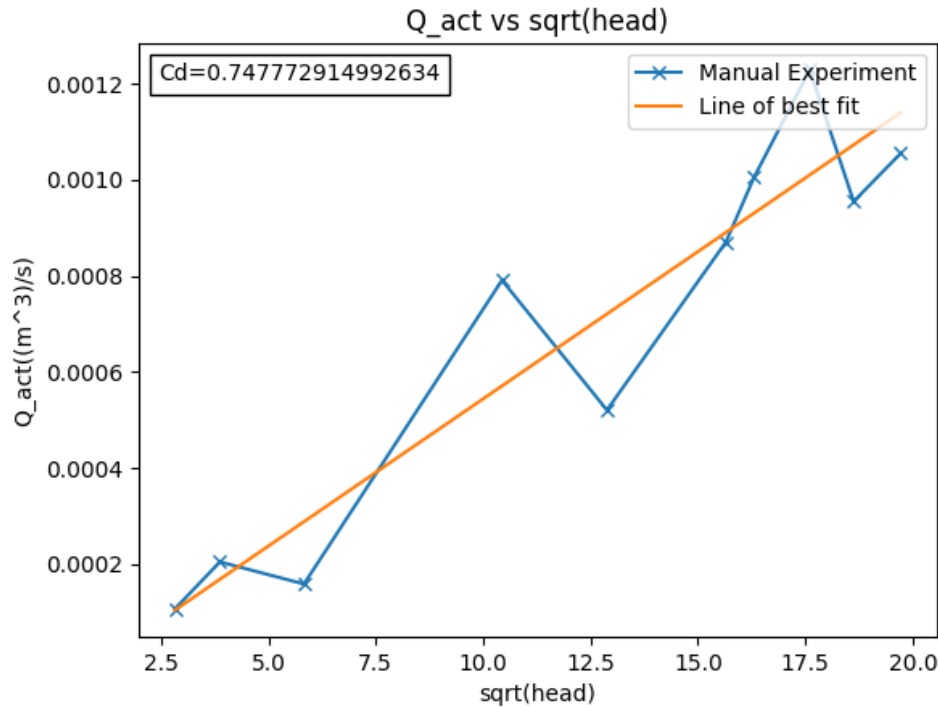


Figure 4.8: Manual Experiment

#### 4.6.2 Experiment 1

The results from the second experiment are tabulated in table 4.2 below.

Table 4.2: Experiment 1

Step 1	Height 1	Height 2	Head	Weight 1	Weight 2	Weight	Temperature(deg. C)	Time
0	390	390	0	5.61	5.61	0	24.5	
1	390	375	15	5.61	12.2	6.59	23.62	38
2	365	345	20	5.14	12.56	7.42	23.38	34
3	315	280	35	5.36	15.94	10.58	23.44	30
4	287	237	50	5.76	18.45	12.69	23.5	26
5	244	188	56	5.79	19.05	13.26	23.5	23
6	205	133	72	5.79	18.7	12.91	23.56	19
7	177	90	87	5.75	17.64	11.89	23.5	15
8	150	59	91	5.75	16	10.25	23.62	12
9	135	29	106	5.74	13.6	7.86	23.56	8
10	116	3	113	5.67	11	5.33	23.56	4

The coefficient of discharge  $C_d$  from the graph of the actual flow rate ( $Q_{\text{act}}$ ) versus the

square root of was found to be as shown in figure 4.9. The  $C_d$  from experiment 2 was however way below the actual  $C_d$  with a percentage error of approximately 15 percent.

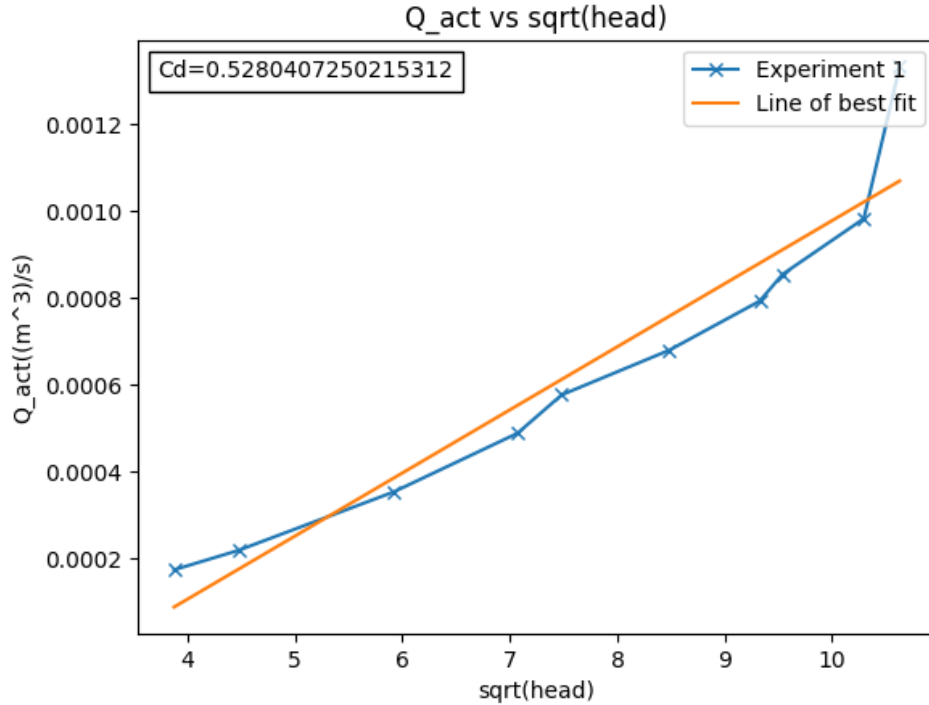


Figure 4.9: Experiment1

### 4.6.3 Experiment 2

The results from the third experiment are shown in table 4.3

Table 4.3: Experiment 2

Step	Height 1	Height 2	Head	Weight 1	Weight 2	Weight	Temperature(deg. C)	Time
0	410	410	0	6.13	6.13	0	22.5	
1	375	360	15	6.13	14.34	8.21	22.94	38
2	359	342	17	6.01	15.9	9.89	23.06	34
3	330	295	35	6.11	18.85	12.74	23.12	30
4	295	243	52	6.11	20.55	14.44	23.19	27
5	256	185	71	6.11	21.25	15.14	23.19	23
6	214	119	95	6.2	21.05	14.85	23.25	19
7	192	56	136	6.13	21.25	15.12	23.25	15

Figure 4.10 depicts the coefficient of discharge (0.76198) from the second round.

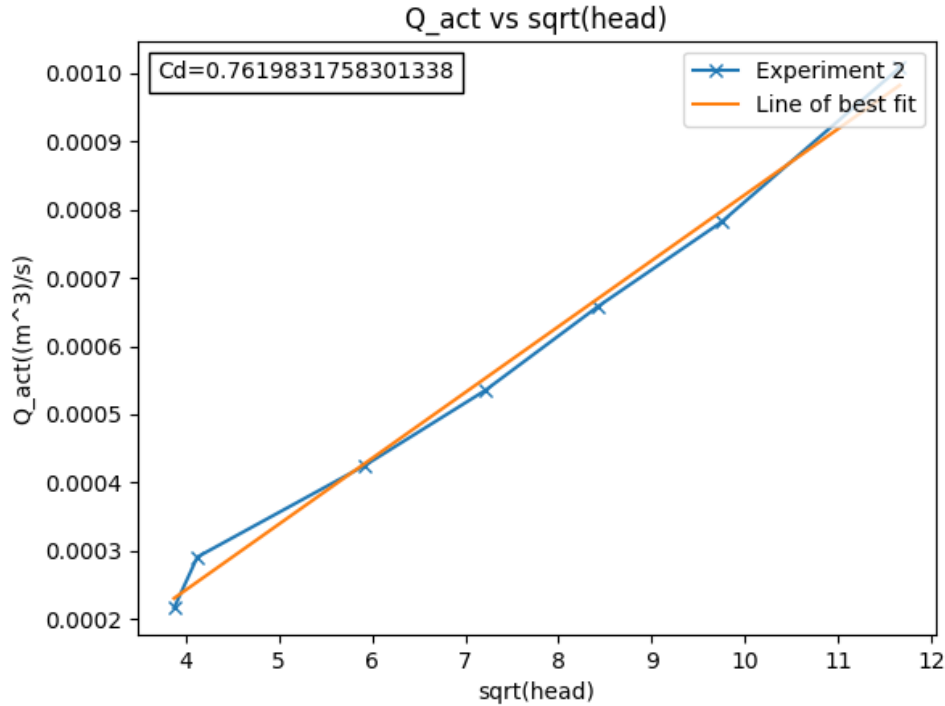


Figure 4.10: Experiment2

#### 4.6.4 Experimnet 3

The results from the third run are illustrated in table 4.4.

Table 4.4: Experiment 3

Step	Height 1	Height 2	Head	Weight 1 (kg)	Weight 2 (kg)	Weight	Temp (degrees)	Time
0	327	327	0	6.28	6.28	0	21.81	
1	275	265	10	6.28	16	9.72	21.88	48
2	250	231	19	5.28	18.23	12.95	22	43
3	205	165	40	5.39	21.72	16.33	22.12	38
4	157	105	52	5.39	23.1	17.71	22.19	33
5	121	56	65	5.41	22.95	17.54	22.19	28
6	88	13	75	5.4	21.67	16.27	22.25	23

The graphical illustration of a graph of the actual flow rate ( $Q_{\text{act}}$ ) versus the square root resulted in the final coefficient of discharge of 0.82175. Compared to the results from the manual experiment, there was a 8.213 % percent reduction in the overall error.

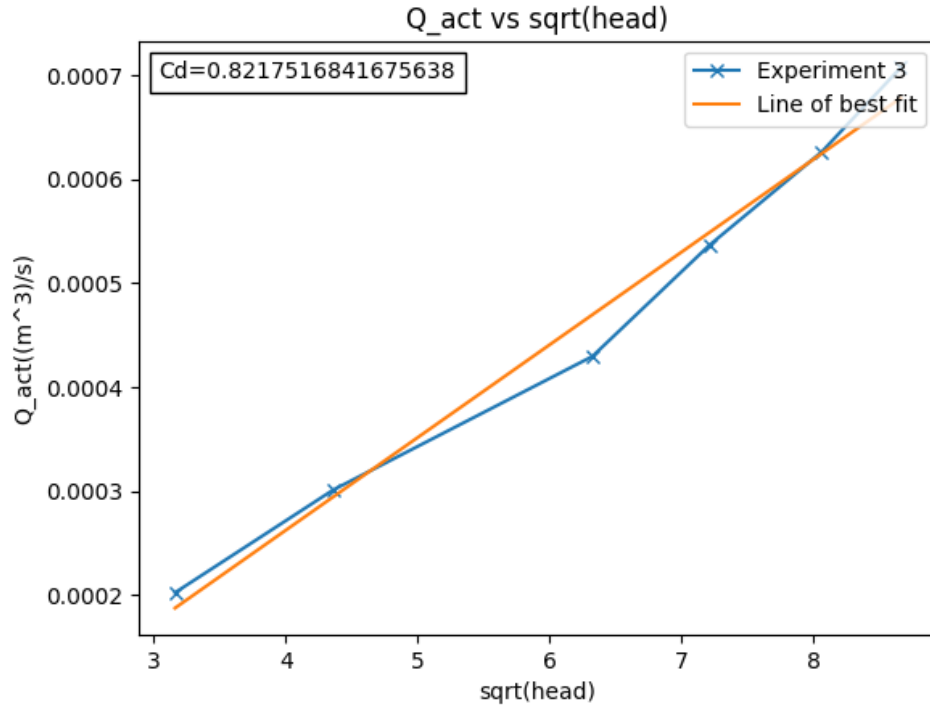


Figure 4.11: Experiment3

The system reduced the overall human error margin that arises from the manual operation of the experiment by approximately 10 percent as depicted from the values obtained in the second and final run of the experiment. The calculations were based on the average coefficient of discharge of the venturi, 0.985. The first automatic run was however not as successful as anticipated. This was because of the very high-pressure discharge from the main pipeline that strained the LA-T8 electromagnet linear actuator leading to delays in discharge diversion and thus incorrect readings. The pressure was however adjusted to the required level.

## 5 Conclusion

The design and development of an automated discharge collection for the synthetic hydro experimental machine were fully realized. This project had three specific objectives;

- To design an automated discharge flow control mechanism that could turn the ball valve in steps of less than a degree
- To design and fabricate a discharge handling mechanism incorporated with automatic weight, time, and temperature measurement
- To design a graphical user interface along with a robust control algorithm to integrate all the unit

All three objectives were fully met. For the first objective, the system could precisely control the flow rate in the required step as input from the user interface. For the second objective, the discharge handling mechanism was able to divert the discharge as intended. Furthermore, the weight and temperature measurement units were able to record and send correct real-time values into the user interface for display. Finally, a graphical user interface was realized that could allow for both manual and automatic operation of the machine. The system could further be able to communicate to the desktop graphical user application via Ethernet support.

### 5.1 Recommendation

- The system can be made fully automated by incorporating a  $1\frac{1}{2}$  inch solenoid valve or a series of  $\frac{1}{2}$  inch solenoid valves to reduce on time taken when emptying the tank. Digital barometric pressure sensors can also be used in place of the manometer.

## References

- [1] M. Pereira, “Flow meters: part 1,” *IEEE Instrumentation & Measurement Magazine*, vol. 12, no. 1, pp. 18–26, 2009.
- [2] P. Nandagopal and S. Nuggenhalli, “Fluid flow measurements,” pp. 137–147, 2022.
- [3] R. K. Raman, Y. Dewang, and J. Raghuwanshi, “A review on applications of computational fluid dynamics,” *International Journal of LNCT*, vol. 2, no. 6, pp. 137–143, 2018.
- [4] A. Tukimin, M. Zuber, and K. Ahmad, “Cfd analysis of flow through venturi tube and its discharge coefficient,” in *IOP Conference Series: Materials Science and Engineering*, vol. 152, no. 1. IOP Publishing, 2016, p. 012062.
- [5] M. Carello, A. Ivanov, and F. Pescarmona, “Flow rate test bench: automated and compliant to iso standards,” *Experimental Techniques*, vol. 37, no. 2, pp. 41–49, 2013.
- [6] N. Tamhankar, A. Pandhare, A. Joglekar, and V. Bansode, “Experimental and cfd analysis of flow through venturimeter to determine the coefficient of discharge,” *International Journal of Latest Trends in Engineering and Technology (IJLTET)*, vol. 3, no. 4, pp. 194–200, 2014.
- [7] “Venturi Flowmeter.” [Online]. Available: <http://hyperphysics.phy-astr.gsu.edu/hbase/Fluids/venturi.html>
- [8] R. Arun, K. Yogesh Kumar, and V. Seshadri, “Prediction of discharge coefficient of venturimeter at low reynolds numbers by analytical and cfd method,” *International Journal of Engineering and Technical Research (IJETR) ISSN*, pp. 2321–0869, 2015.
- [9] A. Odetti, G. Bruzzone, M. Caccia, R. Ferretti, E. Spirandelli, and G. Bruzzone, “Design, development and testing at field of a modular mini automatic water sampler (maws) based on magnetic activation,” in *OCEANS 2019-Marseille*. IEEE, 2019, pp. 1–8.

- [10] S. Lee and J. Kim, “Development and characterization of a cartridge-type pneumatic dispenser with an integrated backflow stopper,” *Journal of Micromechanics and Microengineering*, vol. 20, no. 1, p. 015011, 2009.
- [11] “MG996R Servo Motor.” [Online]. Available: <https://components101.com/motors/mg996r-servo-motor-datasheet>
- [12] “D8120 Datasheet, PDF - Alldatasheet.” [Online]. Available: <https://www.alldatasheet.com/view.jsp?Searchword=D8120&sField=3>
- [13] “LA-T8 linear actuator,Max 150mm/s speed,235N,150mm stroke,Hall sensor.” [Online]. Available: [http://www.gomotorworld.com/pd?product\\_id=64&brd=1](http://www.gomotorworld.com/pd?product_id=64&brd=1)
- [14] “Getting Started with Load Cells - learn.sparkfun.com.” [Online]. Available: <https://learn.sparkfun.com/tutorials/getting-started-with-load-cells/all>
- [15] “DS18B20 Temperature Sensor.” [Online]. Available: <https://components101.com/sensors/ds18b20-temperature-sensor>
- [16] “Black STM32 F407VE Development Board — Zephyr Project Documentation.” [Online]. Available: [https://docs.zephyrproject.org/3.1.0/boards/arm/black\\_f407ve/doc/index.html](https://docs.zephyrproject.org/3.1.0/boards/arm/black_f407ve/doc/index.html)

## A Appendix

### A.0.1 Budget

Table A.1: Budget

Item No	Item	Description	Unit cost	Qty	Total Cost
1	Servo Motor	DS8120(20Kg/cm)	2500	1	0
2	Linear Actuator	LA-T8 Linear Actuator	3500	1	3500
3	Load cells	50 Kg Load cells	150	4	600
4	Load cell Amplifier	HX711	100	1	100
5	Temperature Sensor	DS18B20 Immersible	300	1	300
6	Ball valve	1 1/2" Plastic valve	1650	1	1650
7	MCU	STM32F407VET6	4400	1	4400
8	LCD	320x240 Touch LCD	1200	1	1200
9	4 Pole relay	4 Pole relay	400	1	400
10	Voltage regulator	XL4015 DC-DC adjustable buck module	400	3	1200
11	Transformer	AC 220V TO DC 12V 5A Transformer Power Supply	1100	1	1100
12	Ethernet Module	W5500 Ethernet module	720	1	720
12	Fabrication Cost	3D printing & Others	4000	1	4000
13	Miscellaneous	Miscellaneous	800	1	800
Total					<b>19970</b>

### A.0.2 Computation of the coefficient of discharge of the venturi meter

```

1 import pandas as pd
2 import numpy as np
3 from matplotlib import pyplot as plt
4 from matplotlib.offsetbox import AnchoredText
5
6 df = pd.read_excel('../ManualExperiment.xlsx')
7 height_diff = df['Head'].to_numpy()
8 weight_diff = df['Weight'].to_numpy()
9 time_s = df['Time'].to_numpy()
10
11 # Remove the first row of the arrays
12 height_diff = height_diff[1:]
13 weight_diff = weight_diff[1:]
14 time_s = time_s[1:]
15 d1 = 35 # entry point diameter
16 d2 = 23 # exit point diameter
17 A1 = (np.pi/4) * (d1*d1)
18 A2 = (np.pi/4) * (d2*d2)
19

```

```
20 weight_m3 = weight_diff /1000 # weight in m^3
21 Q_act = weight_m3/time_s
22 Q_th = A1 * A2 * (np.sqrt((2 * 9.81 * height_diff)) / np.sqrt( (A1*A1) *
23 (A2 * A2)))
24 height_sqrt = np.sqrt(height_diff)
25
26 # compute the slope and intercept
27 slope, intercept = np.poly1d(np.polyfit(np.log10(Q_act), np.log10(
28     height_sqrt), 1))
29 # plot Q_act vs height_sqrt
30
31 plt.title('Q_act vs sqrt(head)')
32 plt.xlabel('sqrt(head)')
33 plt.ylabel('Q_act((m^3)/s)')
34
35 a1 = AnchoredText("Cd={}".format(slope), loc=2, pad=0.4, borderpad=0.5)
36 plt.gca().add_artist(a1)
37
38 plt.plot(height_sqrt, Q_act, label='Manual Experiment', marker='x')
39 plt.plot(np.unique(height_sqrt), np.poly1d(np.polyfit(height_sqrt, Q_act
    , 1))(np.unique(height_sqrt)), label='Line of best fit')
40 plt.legend(loc='upper right')
41 plt.savefig('Manual_Exp.png')
```

Listing 1:  $c_d$  computations

**A.0.3 Semester 1 & 2 Time Plan**

Week	1	2	3	4	5	6	7	8	9	10	11
Project proposal											
Continuous Presentation											
Literature review											
Discharge flow control design											
Discharge collection unit design											
Interface and control design											
Assembly and testing											
Interim report											
Final presentation											

Table A.2: Semester 1 timeplan

Table A.3: Semester 2 Timeplan

Table A.4: Production Plan

Week	Tasks/Activities	Materials Required	Special Equipment	Simultaneous Activity	Status
1	Main activity a) Ordering.	Acquisition of materials Poly-Arctic Acid(PLA)		Design for production	Done
2	Main activity b) Scraps 3D Printing(Discharge Flow Control)	Stainless Steel sheet PLA	3D printer	Circuit Assembly GUI Development	Done
	b) MG996R Servo motor holder	PLA			
	c) Mounting rods	PLA			
	d) Interface	PLA			
	e) Nuts	PLA			
3	Main activity 3D Printing(Discharge Diversion)	PLA	3D printer	Circuit Assembly GUI Development	Done
	a) LA-T8 Holder	PLA			
	b) Diversion support	PLA			
	c) Straps	PLA			
	d) Nuts	PLA			
	e) Flap holder	PLA			
	f) Flap	PVC			
4	Main activity Collection tank fabrication			Firmware development	Done
	a) Frame support	Mild Steel brackets	Welding machine		
	b) Tank	Stainless Steel sheet	Rolling machine		
5	Main activity Mechanical assembly on site			Firmware development	Done
	a) Flow control				
	b) Flow diversion				
	c) Discharge handling				
6	Main activity Electrical Assembly				Done
	a) Circuit development				
	b) Circuit Assembly				
7	Main activity Final Assembly and calibration			Testing	Ongoing
	a) Calibration				
	b) Testing				
	c) Ethernet Support				
	d) Tank fabrication				
8	Main activity Ethernet Support			Troubleshooting	Done
	a) Desktop GUI				
	b) Ethernet - Black_E407ve conn.				
9	Main activity Testing		Hydraulic Test rig		Done
	a) Units testing				
	b) Experiments				
	c) Data Analysis				
10	Main activity Drafting report specs.				Done
11	Main activity Report writing				Done
12	Main activity Presentations				